Amoeboid Cells as a Transport System for Micro-Objects

Oliver Nagel

June 1, 2019

Oliver Nagel
Amoeboid Cells as a Transport System for Micro-Objects
Dissertation zur Erlangung des akademischen Grades
doctor rerum naturalium (Dr. rer. nat.), June 1, 2019
Reviewers: Carsten Beta , Svetlana Santer and Till Bretschneider
Supervisors: Carsten Beta and Stefan Klump

University of Potsdam
Biological Physics
Institute of Physics and Astronomy
Karl-Liebknecht-Str. 24/25
14476 Potsdam

https://doi.org/10.25932/publishup-44219
https://nbn-resolving.org/urn:nbn:de:kobv:517-opus4-442192

University of Potsdam

Institute of Physics and Astronomy
Biological Physics

Dissertation zur Erlangung des akademischen Grades
doctor rerum naturalium (Dr. rer. nat.)

Amoeboid Cells as a Transport System for Micro-Objects

Oliver Nagel

1. Reviewer Carsten Beta
Biological Physics
University of Potsdam

2. Reviewer Svetlana Santer
Experimental Physics
University of Potsdam

3. Reviewer Till Bretschneider
Experimental Physics
University of Warwick

Supervisors Carsten Beta and Stefan Klumpp

June 1, 2019

Oliver Nagel
Amoeboid Cells as a Transport System for Micro-Objects
Dissertation zur Erlangung des akademischen Grades
doctor rerum naturalium (Dr. rer. nat.), June 1, 2019
Reviewers: Carsten Beta , Svetlana Santer and Till Bretschneider
Supervisors: Carsten Beta and Stefan Klumpp

University of Potsdam
Biological Physics
Institute of Physics and Astronomy
Karl-Liebknecht-Str. 24/25
14476 Potsdam

Abstract

Due to advances in science and technology towards smaller and more powerful processing units, the fabrication of micrometer sized machines for different tasks becomes more and more possible. Such micro-robots could revolutionize medical treatment of diseases and shall support to work on other small machines. Nevertheless, scaling down robots and other devices is a challenging task and will probably remain limited in near future. Over the past decade the concept of bio-hybrid systems has proved to be a promising approach in order to advance the further development of micro-robots. Bio-hybrid systems combine biological cells with artificial components, thereby benefiting from the functionality of living biological cells. Cell-driven micro-transport is one of the most prominent applications in the emerging field of these systems. So far, micrometer sized cargo has been successfully transported by means of swimming bacterial cells. The potential of motile adherent cells as transport systems has largely remained unexplored.

This thesis concentrates on the social amoeba *Dictyostelium discoideum* as a potential candidate for an amoeboid bio-hybrid transport system. The use of this model organism comes with several advantages. Due to the unspecific properties of *Dictyostelium* adhesion, a wide range of different cargo materials can be used for transport. As amoeboid cells exceed bacterial cells in size by one order of magnitude, also the size of an object carried by a single cell can also be much larger for an amoeba. Finally it is possible to guide the cell-driven transport based on the chemotactic behavior of the amoeba. Since cells undergo a developmentally induced chemotactic aggregation, cargo could be assembled in a self-organized manner into a cluster. It is also possible to impose an external chemical gradient to guide the amoeboid transport system to a desired location.

To establish *Dictyostelium discoideum* as a possible candidate for bio-hybrid transport systems, this thesis will first investigate the movement of single cells. Secondly, the interaction of cargo and cells will be studied. Eventually, a conceptional proof will be conducted, that the cheomtactic behavior can be exploited either to transport a cargo self-organized or through an external chemical source.

Zusammenfassung

Durch die Fortschritte in Wissenschaft und Technik hin zu kleineren und leistungsfähigeren Prozessoren wird die Herstellung von Maschinen mit einer Größe von wenigen Mikrometern immer wahrscheinlicher. Solche Mikro-Roboter könnten sowohl die medizinische Behandlung von Krankheiten revolutionieren als auch dabei helfen andere kleine Maschinen zu bauen. Nichts desto trotz ist es eine komplizierte Aufgabe Roboter sowie andere Maschinen zu verkleinern und wird in naher Zukunft wohl nur begrenzt möglich sein. Im Verlauf des letzten Jahrzehnts hat sich das Konzept der Bio-Hybridsysteme als ein vielversprechender Ansatz entwickelt, um Mikro-Roboter weiter zu entwickeln. Bio-Hybridsysteme kombinieren biologische Zellen mit künstlichen Komponenten, um so einen Vorteil aus der Funktionalität lebender biologischer Zellen zu ziehen. Der zellgetriebene Mikro-Transport ist eine der bekanntesten Anwendungen in dem wachsenden Feld dieser Systeme. Bisher wurde mikrometergroße Fracht erfolgreich mit Hilfe von schwimmenden Bakterien transportiert. Das Potential beweglicher, adhärenter Zellen als Transportsystem blieb bisher weitgehend unerforscht.

Diese Arbeit beschäftigt sich mit der sozialen Amöbe *Dictyostelium discoideum* als einen potentiellen Kandidaten für ein auf Amöben basiertes Bio-Hybridtransportsystem. Die Nutzung dieses Modellorganismus bringt einige Vorteile mit sich. Auf Grund der unspezifischen Adhäsion von *Dictyostelium* ist es möglich eine Vielzahl von verschiedenen Frachtmaterialien für den Transport zu nutzen. Da Amöben um eine Größenordnung größer sind als Bakterien, können auch die Objekte, die eine einzelne Amöbe transportieren kann um einiges größer sein, als bei einer einzelnen Bakterie. Desweiteren ist noch möglich den zellgetrieben Transport durch das chemotaktische Verhalten der Amöben zu steuern. Da die Zellen im Verlauf ihres Lebenszyklus' eine entwicklungsinduzierte chemotaktische Aggregation durchlaufen, ist es möglich, die Fracht in einer selbstorganisierten Art und Weise in Aggregate zusammen zu führen. Es ist auch möglich einen externen chemotaktischen Stimulus zu generieren, um das auf Amöben basierende Transportsystem zu einer gewünschten Position zu lenken.

Um *Dictyostelium discoideum* als denkbaren Kandidaten für ein Bio-Hybridtransportsystem zu etablieren, wird in dieser Arbeit zuerst die Bewegung einzelner Zellen untersucht. Als zweites wird die Interaktion von Zellen und Fracht studiert. Zum Schluss wird ein konzeptioneller Beweis geführt, dass das chemotaktische Verhalten der Zellen genutzt werden kann, um eine Fracht entweder selbstorganisiert oder mit Hilfe eines externen Stimulus zu transportieren.

Contents

1

Introduction

The delivery of drugs, that overcomes the limitations of conventional drug management, is an important field in healthcare [1]. Several developments for prevention and treatment of diseases have been devoted over the past two decades [2]. The demand to develop inventive strategies for enhancing delivery efficiency of the therapeutic agents has been rapidly increasing. Over the past two decades, research has been devoted to several developments in this upcoming technology segment for prevention and treatment of diseases [3]. It is especially of interest to minimize side effects, decrease the frequency of drug intake and to improve the *in vivo* drug stability [3]. Especially in cancer therapeutics target drug delivery based on nano-particles has attracted great attention [4] The drug delivery based on nano-technology delivers drug loaded nano-particles to a target site. These strategies are divided into two categories: active and passive ones. Passive strategies accumulate the drug at the disease site through enhanced permeation and retention effects. Unfortunately, most of the nano-particles (more than 95%) accumulate in other organs than the targeted one, causing side effects. The active strategy, on the other hand, depends on specific interaction between the target and the drug load. This occurs only in close range of approximately 5 nm. Since nano-particles lack the ability to propel them self towards the target the targeting efficiency is quite low [4]. To overcome this problems the application of a micro-robot as a delivery agent could be used.

Unfortunately, it is a challenging task to scale down robots and other devices depends on developing reliable and efficient power sources, sensors and actuators [5]. As a result the use of micro-robots will probably remain limited in near future. A promising approach to overcome the problems with the fabrication of micro-robots is the concept of bio-hybrid systems. Bio-hybrid systems combine biological cells with artificial components, taking advantage of the functionality of living biological cells. The energy conversion efficiency is orders of magnitudes greater for biological motors compared to the existing non-biological micro-motors [6]. The most prominent application in this emerging field is the cell-driven micro-transport. So far, micrometer sized cargo has been successfully transported with the help of swimming bacterial cells [7–9]. The potential of motile adherent cells as transport systems has remained unexplored.

Motile adherent cells like amoebic cells could be used complimentary to swimming bacteria. As amoebas exceed the size of bacteria by one order of magnitude also the size of the cargo carried by a single cell can be bigger than for bacteria. Another advantage is that the influence of perturbations of an advective flow is smaller on adherent cells, as their movement is based on substrate adhesion. For medical applications it is also important to know that the leukocytes inside the human body are motile adherent cells as well, this makes them the ideal candidate for in-body use.

This thesis studies the social amoeba *Dictyostelium discoideum* as a potential candidate for an amoeboid bio-hybrid transport system. *Dictyostelium* is a well studied model organism for amoeboid movement and chemotaxis. Due to its' unspecific adhesion properties, it can be used to transport a wide range of different cargo materials. During the life cycle of *Dictyostelium* it undergoes a developmentally induced chemotactic aggregation, cargo could be assembled in a self-organized manner into a cluster. Furthermore, it is also feasible to impose an external chemical gradient to guide the amoeboid transport system to a desired location.

In the next two chapters the reader will be provided with the basic knowledge to understand this work and introduced into the methods used in the different experiments and analysis.

Chapter 4 represents the main results of the thesis. At first the movement of cells without cargo should be studied in more detail. Next the transport of a single particle by a single cell will be analyzed and compared to the movement of single cells. Furthermore, this thesis will try to address the forces exerted by a single cell on the particles. Finally, cells will be guided via chemotaxis to transport cargo to a specific place.

The last two chapters discuss the results in the light of previous research and give a small conclusion of this work. Furthermore, the reader will get a brief outlook of possible future research topics.

Background

2

2.1 Bio-Hybrids

The aim of this thesis is to establish a new bio-hybrid system. Therefore, this chapter will give an introduction to this topic and show the current stat of the art in this field. Furthermore, advantages and disadvantages of the current systems will be displayed and how a new bio-hybrid system could overcome some of these limitations.

During the last decades, technology has made tremendous progress in developing micro-machines. It is possible to transport millimeter sized objects by micro-robots [10] and micro-swimmers can reach velocities comparable to living cells [11]. Nevertheless constructing reliable micro-robots is still a challenging task. Among all the problems, the greatest challenges in creating mobile robots and devices on the micrometer scale are to developing reliable and efficient actuators, sensors, and power sources [5]. Mirco-robots are often driven by a large scale external system such as powerful magnetic coils. Another approach is micro-robots driven by fuels, such as hydrogen peroxide. Unfortunately the regulation of the environment of fuel-driven systems often needs to be precise. Furthermore fuel-driven micro-machines can produce toxic byproducts, like the toxic inorganic ions generated from the corrosion of catalytic metallic motors [12].

A possible solution to overcome these problems is the merging of artificial micro-objects and biological cells to a so-called bio-hybrid system. Living cells developed over millions of years and the energy conversion efficiency are orders of magnitudes higher than that of artificial micro-motors [6]. Furthermore, living cells are able to perform chemotaxis, phototaxis and even magnetotaxis, which allow to control and guide the cells. Different forms of bio-hybrid systems exist. One use of bio-hybrids is the building of simple micro-actuators. An example of such a micro-actuator is the development of a spherical hart-like pump, driven by rat cardiomyocytes [13]. Also smooth muscle cells of rats could be used to build a bio-micro-actuator. The displacement of the pillars could be controlled by chemical stimuli [14]. Micro-actuators can be developed further to micro-manipulators. Therefore, muscle cells are either span between the gripper arms or coated onto them. Such grippers have been fabricated for example out of PDMS [15, 16] or even out of dog hair[17]. In 2013 the first atmospheric-operable bio-hybrid gripper has been developed by

Akiyama and co workers. It was driven by insect dorsal vessel tissue, which was capsuled in 40 μL of culture medium. Under the right conditions the gripper was able to operate for more than five days [18]. Besides using cells to power micro-manipulators they can also been used to grind small gears. In one of the first attempts the gliding bacteria *Mycoplasma mobile* was used to drive a silicon dioxide rotor with a diameter of 20 μm. The bacteria had been glued to the rotor through biotin-streptavindin interactions. The rotor rotated with 1.5-2.6 rpm [19]. Later rotation rates of up to 24.2 rpm have been achieved, by swarming *Vibrio alginolyticus* colliding with the 2 μm thick and 20 μm diameter gear [20]. It is also possible to convert the mechanical energy generated by the cells into electrical power and build a small micro-power generator. To build such a generator the flagella of *E. coli* cells had been adhered to a substrate that way that the cell bodies were free to rotate. To harness the energy out of the rotation ferromagnetic beads had been attached to the cell body. The rotating magnetic field was converted to electric energy using copper coils [21]. With the help of micro-organisms it is also possible to transport small cargo by building a bio-hybrid transport system. The bio-hybrid transport approach developed from first proof of concept studies [7] to a combination of the advantages of non-biological and biological micro-systems [8]. In 2005 Douglas B. Weibel and coworkers showed, that it is possible to guide bio-hybrids, composed of *Chlamydomonas reinhardtii* and polymer beads with a diameter of 6 μm, with the help of light with a wavelength of 500nm [7]. In 2015 the flagellated bacteria *Salmonella typhimurium* was combined with 5 to 10 μm big micro-beads, which contain magnetic particles. It was shown, that this type of system can be guided by a combination of a magnetic field and a chemical gradient [8]. Furthermore, in 2017 the magnetotactic bacteria *Magnetosopirrillum gryphiswalense* were adhered inside mesoporous silica micro-tube to carry antibiotics towards an *E.coli* bio-film. To guide the system towards the bio-film a magnetic field was used [9]. In the past it was already possible to use bio-hybrid systems to transport fluorescent particles inside a mouse towards a tumor. Therefore, rhodamine-containing fluorescent carboxylated PS micro-beads were coupled to *Salmonella typhimurium*. The bacteria acted chemotactic towards the tumor cells, resulting in a delivery of the fluorescent particles inside the tumor [22]. To compare the different transport systems the speed is measured in body length per second (BLPS). The system introduced by Weibel and co-workers for example reached up to 12 BLPS. Another way to compare the transport system is to compare the target to cell size ratio. In the case of the bio-hybrid system of Weibel it is 0.3 [7]. Although, the concept of bacteria for drug delivery seems promising it comes with some serious problems as bacteria themselves are often a reason for infection. The use of bacteria has to be fine tuned to cause not more harm than help for the body [23].

Most bio-hybrid transport systems presented in the literature make use of swimming bacteria as driving element. Although eukaryotic cells have been used as actuators or micro-manipulators in bio-hybrid systems, their potential to drive micro-transport has not been systematically studied to date.

2.2 Cell Motility and Chemotaxis

The movement of a bio-hybrid system is bound to the principals of cell motility. Therefore, this section will explains the fundamentals of cell motility. Furthermore, chemotaxis will be explained as it can be exploited to guide cells and bio-hybrid system to a certain position.

The migration of cells plays an important role in different biological processes. They can be as simple as the search for food or more complex like the development of an embryo. For this purpose many different ways of migration have been developed like swimming and gliding. This work is focused on amoeboid motion, a wide spread form of eukaryotic cell motility [24].

2.2.1 Amoeboid Motion

In a lab amoeboid cells are mostly studied on 2-D surfaces, where they move by crawling on solid substrates. This process can be divided into three steps as displayed in figure 2.1. At first, a membrane protrusion is formed which is also called a pseudopod. The protrusion grows and attaches to the surface. Then, the rear end of the cell detaches and retracts following the pseudopod [25]. It is generally assumed that the cytoskeleton generates the required force to drive this process [26]. The important force generating entities are polar actin filaments [27]. In a tread milling process, constantly adding actin monomers to the barbed ends of the filaments while disassembling actin monomers at the pointed ends simultaneously, a dense dynamic network is formed at the leading edge of the cell [28]. If the filaments of this network grow by polymerization against the plasma membrane, the resulting force drives the formation of a pseudopod. Another important cytoskeletal protein is myosin II. This motor protein is mostly located at the sides and at the rear end of the cell, as it plays a key role in contraction of the cell cortex [29].

2.2.2 Chemotaxis

Chemotaxis, the directed motion in a chemical gradient, plays an important role for a number of processes, for example, wound healing, axon guidance, or the search for food of single-celled organisms [31]. During chemotaxis the cell orients itself and starts to polarize along the gradient. For detection of the gradient receptors

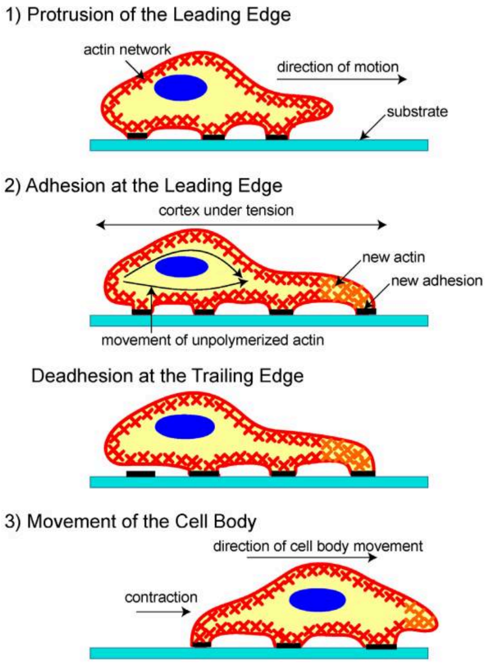

Fig. 2.1: The steps of amoeboid motion. First, the actin network forms a pseudopod at the leading edge of the cell. Second, the new formed pseudopod attaches to the ground while the rear end detaches from the ground. Last, the rear of the cell contracts and a new pseudopod is formed. Taken from [30]

are distributed over the cell membrane. Interestingly, the chemotactic machinery in many eukaryotic cell types is controlled by a highly conserved transduction pathway, although the organisms themselves have evolutionary separated long ago, such as *Dictyostelium discoideum* and mammalian neutrophils [32]. In *Dictyostelium*, one of the best studied model organisms of chemotaxis, gradient induced directional motion can be observed during growth and development. Chemotaxis of *Dictyostelium* is discussed in more detail in section 2.3.1.

For sensing chemical gradients cells can use two different strategies: temporal sensing or spatial sensing. Cells performing temporal sensing compare the receptor activity at different times and adapt their movement to this information. *E. coli* for example, a bacterium that moves in a sequence of straight runs and random turns and uses temporal sensing for exploring the environment, enhances its run time when the concentration of the chemoatractant is increased over time [33]. In contrast cells, using spatial sensing, measure the activity of the receptors over the whole body simultaneously. The different receptor signals trigger a signaling cascade inside the cell, leading to polarization of the cell and migration towards the chemoatractant. For a more detailed description of this process in *Dictyostelium* the interested reader is referred to 2.3.2. The process of spatial sensing in *Dictyostelium* ranges from shallow signals close to the noise level to steep gradients and high offset concentrations [34]. The cellular response to the signal can be described with help of a biased excitable network combined with a local excitation - global inhibition system [35]. If the receptors in one part of the membrane are activated, the probability of pseudopod formation in this region will be increased; meanwhile the probability of pseudopod formation over the rest of the membrane is being reduced.

2.2.3 Random Walk Models

This chapter will provides the reader with a brief introduction to random walk processes in nature and will explains the basics of the physical concept. This helps the reader to understand the findings in chapter 4.1, which deals with the movement statistics of vegetative *Dictyostelium discoideum* cells.

In 1828 the botanist Brown observed the irregular movement of pollen particles [36] known as Brownian motion. This process has been described at the beginning of the 20th century as a random walk [37]. Further development on the random walk theory were taken by Uhlenbeck and Ornstein 1930 [38]. Random walk processes can be divided into different groups: The simple isotropic random walk (SRW), the correlated random walk (CRW) and the biased random walk (BRW). The SRW is the simplest case of a random walk. Each step is independent to the previous movements and there is no preferred direction. Thus the location of the particle after each step of the random walk depends solely on the previous position and is therefore Markovian with regards to the location [39]. Using this fact it is a simple task to derive the probability density function (PDF) for one dimension. A walker on an infinite one-dimensional uniform lattice can only be at an even distance away from its origin after an even number of steps. The same rule holds for an odd number of steps. Leading to a binomial distribution for the probability of the walker to be at the position $m\delta$ were m displays the number of steps towards one direction and δ displays the step length after n time steps:

$$p(m,n) = \frac{n!}{2^n \left(\frac{n+m}{2}\right)! \left(\frac{n-m}{2}\right)!} \tag{2.1}$$

For a large number of time steps $t = n\tau$ the function converges to a Gaussian distribution, leading to a normally distributed location with mean 0 and a variance of $\delta^2 \frac{t}{\tau}$. For infinitesimal steps $\delta, \tau \to 0$ this leads to $\frac{\delta^2}{\tau} = 2D$ with the diffusion constant D, resulting in the PDF for the location x of the walker after time t:

$$p(x,t) = \frac{1}{\sqrt{4\pi Dt}} \cdot exp\left(\frac{-x^2}{4Dt}\right) \tag{2.2}$$

This equation also displays the fundamental solution of the diffusion equation.

It is now possible to extend the model to the Fokker-Planck equation and include a drift term [40].

$$\frac{\partial p}{\partial t} = -\nabla \cdot (\vec{u}p) + \nabla \cdot (D\nabla p) \tag{2.3}$$

In this term $\vec{u}$ displays the average drift velocity in x-direction, which is zero, if the walker does not have the possibility to stay at its place.

This drift-diffusion equation is one example of the Fokker-Planck diffusion equation. This equation describes the SRW behavior for $\vec{x} = 0$ and a BRW in case $\vec{x} \neq 0$. Assuming a Dirac delta function $p(\vec{x}, 0) = \delta_d(x_1), \cdot, \delta_d(x_N)$ at the beginning, following PDF results from equation 2.3 [41]:

$$p(\vec{x}, t) = \frac{1}{(4\pi Dt)^{\frac{N}{2}}} \cdot exp\left(\frac{-|\vec{x} - \vec{u}t|^2}{4Dt}\right) \tag{2.4}$$

In this equation N equals the number of dimensions. For N = 1 the equation results in equation 2.2 with an additional drift term. The mean of equation 2.4 is given by $E(\vec{x}_t) = \vec{u}t$ and the square of the mean, also known as mean square displacement (MSD) or variance, is given by:

$$E(|\vec{x}_t|^2) = |\vec{u}|^2 t^2 + 2NDt \tag{2.5}$$

It is interesting to see that for SRW the MSD increases linearly in t while for a BRW it increases for large t linearly in t^2 (ballistic movement) [40, 42].

The movement of animals or cells is directionally correlated or, in other words, persistent. Thus, the SRW and the BRW processes do not fit the previous description. Movement patterns of animals or cells follow the rules of a CRW. In a CRW it is more likely for a walker to keep its direction of movement than to change it. Therefore, this process is no longer a Markovian process [43].

Assuming a cell population on an infinitely long line with a constant speed v either to the left or to the right. The density for individuals moving right at position x and time t is written as $\alpha(x,t)$ and for moving left $\beta(x,t)$ resulting in a total population density $p(x,t) = \alpha(x,t) + \beta(x,t)$. At each time step τ the individual has the possibility to change its direction with the probability $r = \lambda\tau$ or keep the previous direction with the probability $q = 1 - \lambda\tau$ and move a distance δ. Furthermore, it is assumed that $\delta, \tau \to 0$ with $\frac{\delta}{\tau} = v$. Using a Taylor series and the fact that $p = \alpha + \beta$, following equation arises:

$$\frac{\partial^2 p}{\partial t^2} + 2\lambda \frac{\partial p}{\partial t} = v^2 \frac{\partial^2 p}{\partial x^2} \tag{2.6}$$

It is now possible to extent the CRW to two or more dimensions, by adding an up and a down direction, leading to the possible movement directions up (α_u), down (α_d), right (α_r) and left (α_l). These results in an equation for the two-dimensional CRW also known as Fuerth's formula:

$$\frac{\partial^2 p}{\partial t^2} + 4\lambda \frac{\partial p}{\partial t} = v^2 \left(\frac{\partial^2(\alpha_r + \alpha_l)}{\partial x^2} + \frac{\partial^2(\alpha_u + \alpha_d)}{\partial y^2} \right) \tag{2.7}$$

If the initial conditions $p(x,0)$ and $\left(\frac{\partial p}{\partial t}\right)(x,0)$ are given the mean can be calculated to $E(X_t) = 0$ and for the second moment, which is the MSD:

$$E(X_t^2) = \frac{v^2}{\lambda}\left(t - \frac{1}{2\lambda}(1 - e^{-2\lambda t})\right). \tag{2.8}$$

For small t 2.8 converges to $E(X_t^2) \sim v^2 t^2$ under the assumption $t \approx \frac{1}{\lambda}$ holds for small t. While for large t $E(X_t^2) \sim \frac{v^2 t}{\lambda}$. It was shown for the SWR that $D = \frac{\delta^2}{2\tau}$ in one dimension or $D = \frac{\delta^2}{2N\tau}$ for N dimensions. The mean time between turning events can be described as $\bar{\tau} = \frac{1}{\lambda}$ and the average distance between turning events as $\bar{\delta} = \frac{v}{\lambda}$. This relations lead to:

$$D = \frac{\bar{\delta}^2}{2N\bar{\tau}} = \frac{v^2}{2N\lambda} \tag{2.9}$$

Using this relation the MSD of a CRW for large t results in $E(X_t^2) \sim 2NDt$ similar to a SRW. This indicates that a CRW behaves for small time scales ballistic proportional to t^2, while for larger time scales it behaves like a diffusion process proportional to t.

Random walk models can be extended further to a continuous time random walk (CTRW). The theory for CTRW was introduced more than 40 years ago [44]. Each jump in a CTRW process is characterized by a variable waiting time τ after the previous jump and a variable jump length ξ. All τ and ξ are independent variables. The distribution is according to the probability densities $\Psi(\tau)$ and $\lambda(\xi)$. A power law of the form $\Psi(\tau) \simeq \tau^{-1-\beta}$ with $0 < \beta < 1$ results in a diverging waiting time $\int 0 \inf \tau \Psi(\tau) d\tau$. As a consequence the CTRW is sub-diffusive, $\langle r^2(t) \rangle \simeq t^\beta$. For $\lambda(\xi) \simeq |\xi|^{-1-\gamma}$ with $0 < \gamma < 2$ the variance of the jump length $\int - \inf \inf \xi^2 \lambda(\xi) d\xi$ diverges as well, but a super-diffusive Lévy flight is obtained. A coupling of waiting time and jump length leads to Lévy walks with finite $\langle r^2(t) \rangle \simeq t^\beta$ with $1 < \beta < 2$ [45]. The theory of CTRW has already successfully applied in the dispersion of subsurface tracer [46] or in models of gene regulations [47], among many others [48]

It is possible to extend the random walk models further leading to much more complex equations. The interested reader is referred to [49].

In the past different models were used to describe the movement of cells. Based on the observation of the anticorrelation of movement and the periods of turning a detailed model of *Dictyostelium discoideum* locomotion was developed [50]. Furthermore it was shown that it is possible to separate cell motion into a deterministic and a stochastic part. This can be related to physiologically distinct processes [51], and was successfully extended to directional locomotion in a chemical gradient [52]. Also models of fractional Brownian motion have been used to quantify the degree of persistence of *Dictyostelium* cell trajectories [53].

2.3 *Dictyostelium discoideum*

The model organism used in this thesis as a potential candidate for a new bio-hybrid system is *Dictyostelium discoideum*, a social amoeba, which lives in the forest soil. These eukaryotic cells belong to the class of cellular slime molds and are relatively large in sized ($d \approx 10\mu m$).

Dictyostelium discoideum was discovered by K.B. Raper in 1935 [54]. Since then, *Dictyostelium* has become an important model organism for basic bio-medical research in cell and developmental biology. The organism displays many phases of health and diseases, like embryonic development, tumor spreading or the immune response to a disease. These events depend on fundamental processes in individual cells, such as chemotaxis, signal transduction, cytokinesis, motility, and phagocytosis. Furthermore, the full genome has been decoded [55] and there are many mutants available (*http://dictybase.org*), which allow investigations on the role of specific genes in detail.

2.3.1 Lifecycle

In its natural habitat *Dictyostelium* lives on bacteria, which are detected via sensing of folic acid. Moreover, cells were cultured to live and grow in an axenic medium for laboratory work. This procedure proves to be easy to apply.

In absence of a food source *Dictyostelium*, undergoes a characteristic development cycle to form a multi-cellular organism [56]. After several hours in the absence of nutrients, the cells start to release cAMP and also express cAMP receptors. This molecule works as a chemoattractant for *Dictyostelium*. When a cell detects cAMP,

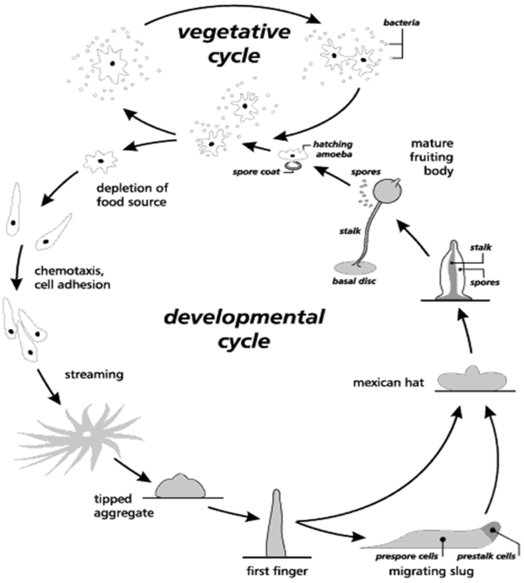

Fig. 2.2: Lifecycle of *Dictyostelium discoideum*: The mature fruiting body is formed after approximately 20 hours of starvation.
Taken from http://www.dictyostelium.com/devcyc.gif

the amoeba changes its shape and reacts in two ways. Firstly it moves up the gradient of cAMP produced by the other cell. Secondly it produces cAMP on its own to enhance the signal, resulting in self-organized cAMP waves traveling throughout the cell population [57]. The production of cAMP as well as the cell movement happens in steps. Every six minutes cAMP is released from cells in the center of the pattern, while the inwardly moving cells follow the gradient upwards. This behavior allows to collect cells from a wide area, which can lead to an aggregate of up to 100,000 cells [57].

It takes the cells about eight hours to collect into a central point. During that time *Dictyostelium discoideum* cells become adhesive and capable to form three-dimensional structures. In this way the aggregate tightens during the next few hours and forms a tip. The tip is an important group of cells that controls further development [56]. It is the source of signals and organizes the behavior of the cells behind the tip. Experiments showed that one can stop the development by cutting it off. The tip leads the cells to form a structure called a finger. The finger can become a migrating slug, wandering around to find food via phototaxis and thermotaxis. Alternatively, the fruiting body is directly produced in place. This process is called culmination. A structure called the Mexican hat is formed and the cells differentiate into prestalk and prespore cells. Afterwards the spore cells move upwards while the stalk cells move downwards in a cellulose tube. The cycle is completed after approximately 20 hours of starvation by formation of the mature fruiting body. It contains the spores in its head, while the stalk cells constitute the stem. If food is restored, the spores can germinate and the cells enter the vegetative cycle again [56]. The whole lifecycle is illustrated in figure 2.2.

2.3.2 Signaling Pathway

When a cAMP molecule binds to the cAR1 receptor of *Dictyostelium* the heteromeric G protein complex ($G_{\alpha 2 \beta \gamma}$), which is linked to the receptor, dissociates into the α and $\beta\gamma$ subunits. Via Ras-signaling the local $G_{\beta\gamma}$ stimulation is transduced through the activation of phosphoinositide 3-kinase (PI3K) at the leading edge [58]. PI3K converts phosphatidylinositol-(4,5)-biphosphate (PIP2) to phosphatidylinositol-(3,4,5)-triphosphate (PIP3). The counterpart to PI3K is phosphoinositide-3-phosphatase (PTEN) which dephosphorylates PIP3. It is mostly localized at the sides and rear end of the cell [59]. Thereby a PIP3 gradient restricted to the front of the cell is established. PIP3 provides a binding side for pleckstrin homology (PH) domain containing proteins like cytosolic regulator of adenylyl cyclase (CRAC), protein kinase B (Akt/PKB), or PH domain carrying protein A (PhdA). CRAC and PhdA are translocated to the front of the cell after the stimulation [60]. CRAC, is also known as a regulator for the adenylyl cyclase, which regulates the cAMP relay, whereas PhdA organizes the F-Actin formation at the front. The activation of Akt/PKB leads to a stimulation and translocation of protein kinase A alpha (PKAa) to the rear end of the cell. PKAa and cGMP, produced by guanylyl cyclase (GC), given that it is activated by the dissociation of the $G_{\beta\gamma}$ subunit, arrange an increase of myosin II phosphorylation and assembly at the back of the cell [61].

Besides this PI3K pathway there are also three other additional known, the phospholipase A2 (PLA2), the soluble guanylyl cyclase (sGC) and the transducer of Regulated CREB protein 2 (TorC2) pathway [63]; [64], shown in figure 2.3. It has been shown that each of these pathways by itself is not essential for chemotaxis. Probably they amplify the ability to sense the gradient and if one of the pathways is knocked out the remaining ones step in to compensate for the loss[62].

2.4 Substrate Adhesion

The studied bio-hybrid system is composed of an amoeboid cell and a polystyrene or silica particle. Except for Some experiments in chapter 4.4.2 where wheat germ agglutinin was used no protein coating is added to the particles to glue them onto the cell. As a result just the natural cell substrate adhesion is exploited for the formation of the bio-hybrid system. This chapter should provide the reader with a basic understanding of this process.

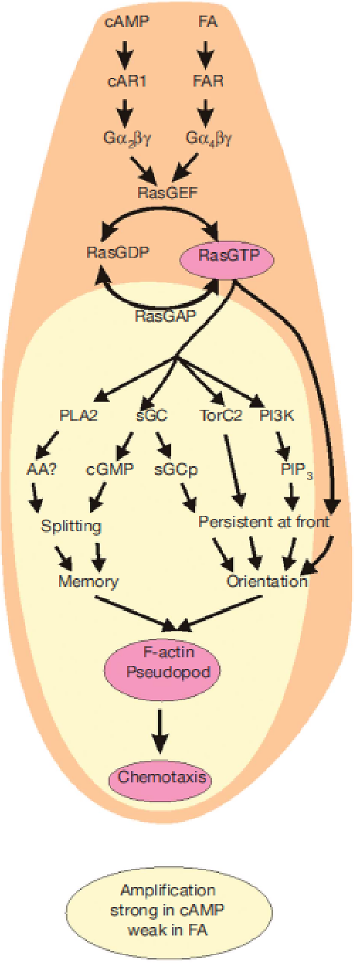

Fig. 2.3: Different chemotactic pathways in *Dictyostelium*. AA, arachidonic acid; FAR, folic acid receptor. Taken from:[62]

The interaction of cells in contact with each other or with their environment is vital for various problems. From the development of multi-cellular organisms over the immune reactions of the human body to cells moving forward, adhesion between cells or cells and an extra cellular matrix (ECM) is relevant. In this work, only adhesion between a cell and a substrate surface is important. This problem is quite well illustrated in standard textbooks [65, 66]. Essential for the interactions of cells with the ECM are the cell adhesion molecules, which form focal adhesion areas. Hence, only parts of the contact area are attached to the surface. An advantage of focal adhesion areas is a faster adjustment of the adhesion strength. For cell movement over a surface it is necessary to build up a strong adhesion at the front and to loosen the attachment at the rear end.

In many motile cells, the focal adhesion points are coupled to the actin network through integrins which are associated with different actin binding proteins e.g. talin, vinculin, paxillin, filamin or α -actinin. The formed focal adhesions remain fixed to the surface till the cell has moved over them [67]. However, the genome of *Dictyostelium* does not include genes for integrins [55]. Therefore, it is obvious that such specialized complexes are not indispensable for substrate adhesion and motility. Although the process of *Dictyostelium* substrate adhesion is not completely understood, a couple of adhesion proteins have been identified. SadA and Phg1 enhance substrate adhesion during the vegetative state of the cell cycle, whereas during development no effect of these proteins has been shown [68, 69]. Another important protein for substrate adhesion is talin. While talin null cells seem to have an adhesion defect during the vegetative state [70] the adhesion is stronger during development compared to wild type cell lines [71]. Furthermore, cell adhesion is enhanced by NapA [72] and proteins of the Sib family, mainly SibA and SibC [73]. Additionally it has been shown, that ampA mediates detachment [74]. Also intracellular signaling proteins like PTEN influence the cell substrate adhesion by regulating the amount of PIP3 at the membrane. PIP3 is necessary to create activated membrane patches and therefore must be highly regulated. It was shown that cells lacking PTEN display a higher level of PIP3 at the membrane and consequently show a higher adhesion [75]. Besides the influence of the different proteins, also Van der Waals forces are significant factors for *Dictyostelium* substrate adhesion [76]. Together all these factors allow *Dictyostelium* cells to move on various surfaces, like naked glass, hydrophobic silinized glass, or hydrophilic serum albumin coated glass [76–78]. This unspecific adhesion is crucial for the cells, as they have to move on very different types of surfaces in their natural surroundings.

2.5 Optical Trap

To establish a new bio-hybrid system it is necessary to know about the characteristics of the system. One important feature is the amount of force a single cell can exert to carry a particle. Chapter 4.3 tries to answer this question. One possible way to measure the forces generated by a single cell is the use of an optical trap. This chapter provides the reader with the basic physical work mechanisms of an optical trap and the limitations of this system.

During the last years the development of optical traps has led to new insights in the bio-sciences. It is feasible to trap cells and bacteria and manipulate them on demand without harming them. The opportunity to apply weak forces from 10 pN up to several hundreds of pN to investigate bacteria/cell adhesion, stretching of bio-polymers or protein-folding forces is important to understand biological matters [79–82]. Although the technique of optical traps is a technique established in the 1980s, basic physics of the method have already known for centuries. Johannes Kepler suggested in the beginning of the 17th century that the tail of comets always points away from the sun because of the radiation pressure. In the 19th century this prediction was verified by a theoretical model of Maxwell. 1986 Arthur Ashkin was the first to trap micrometer sized dielectric particles with a single focused laser beam [83]. Only one year later first organic materials were trapped [84]. For his work he gained the Nobel Prize in 2018.

For trapping particles the light-matter interaction is exploited. The basic principles behind optical trapping have been reviewed several times throughout the years [85–87]. Two different types of forces play a major role the gradient forces and the scattering forces. The gradient forces pull the object toward the laser beams focal point, while the scattering forces push the object along the direction of the laser beam propagation. Furthermore, other factors, like the Stokes' drag force and Brownian motion contribute to the stability of the trap [87]. For isotropic homogeneous spheres the light-matter interaction is based on the relation between particle size and wavelength. This interaction can be divided in three regimes, the geometric optics regime, the Rayleigh regime and the intermediate regime.

In the geometric regime the diameter of the particle is an order of magnitude larger than the laser wavelength. The particle is pulled towards the beam focus by the gradient force generated through the reflection and refraction of light on the particle. The scattering force tends to destabilize the trap in this regime. A light ray traveling in a medium is associated with a linear momentum flux $p = n \cdot \frac{P}{c}$, with P is the power of the ray and n the refraction index of the medium. If a transparent spherical particle experiences this inhomogeneous light field the sum of the momentum flux for the particle that is not at equilibrium within the light field will point away from the region of highest intensity. This causes a gradient force F_{grad} on the sphere along the intensity gradient [83]. The gradient force is accompanied by a scattering force F_{scat} along the optical axis. Reflection and absorption enhance the scattering force. Therefore, it is important that the particle is transparent for the used light ray. A particle can be stably trapped in the light focal point when the gradient force is stronger than the scattering force. This is shown in figure 2.5. In a Rayleigh regime the particle is an order of magnitude smaller than the wavelength. In this case the electric field of the light ray induces a dipole in the particle. Due to the fact that the polarized particle minimizes its energy, it is most stable in the beam focal point because of the present of the high field gradients. In this regime the stability of the trap is strongly influenced by the polarizability of the particle. Harada and Asakura reported 1996 the theoretical expressions of the forces exerted in the Rayleigh regime on a dielectric sphere [88]. For the Rayleigh approximation the dielectric particle is considered to be a volume of infinitesimal point dipoles. This dipoles interact with the electromagnetic field of the light. The induced dipole moment $\vec{p}_d$ can be written as:

$$\vec{p}_d = 4\pi n^2 \epsilon_0 r^3 \left(\frac{m^2 - 1}{m^2 + 2} \right) \vec{E} \tag{2.10}$$

where ϵ_0 is the vacuum permittivity, m is the relative refractive index of the particle, $m = \frac{n_part}{n}$ and $\vec{E}$ is the homogenous electric field. Due to the Lorentz force on the dipole induced by the electric field, the particle will experience the gradient force $\vec{F}_{grad}$:

$$\vec{F}_{grad} = \pi n^2 \epsilon_0 r^3 \left(\frac{m^2 - 1}{m^2 + 2} \right) \nabla |\vec{E}|^2 = \frac{2\pi n \epsilon_0 r^3}{c} \left(\frac{m^2 - 1}{m^2 + 2} \right) \vec{I} \tag{2.11}$$

where $\vec{I}$ is the irradiance. The harmonic oscillation of the electric field in time causes a scattering force $\vec{F}_s cat$. For an incident Gaussian beam it can be written as:

$$\vec{F}_{scat} = \frac{8\pi n k^4 r^6}{3c} \left(\frac{m^2 - 1}{m^2 + 2} \right) \vec{I} \tag{2.12}$$

where k is the wave number $k = \frac{2\pi}{\lambda}$ [88]. The gradient force is the gradient of a scalar function, the trapping potential U

$$U = \frac{2\pi n \epsilon_0 r^3}{c} \left(\frac{m^2 - 1}{m^2 + 2} \right) I \tag{2.13}$$

The trapped particles experience also thermal fluctuations. The kinetic thermal energy of the particle is $k_B T$, with the Boltzmann constant k_B and the absolute temperature T. To stably trap a particle the trapping potential U has to be significantly higher than $k_B T$ [89] In the intermediate regime the particle has a similar size as the laser wavelength. In this case the behavior of the particle is intermediary to the geometric and the Rayleigh regime. It can be modeled by the generalized Lorenz-Mie theories. The mathematical description of a laser beam illuminating a sphere is one of the most challenging tasks in these theories. Most approaches use an analytic approximation of the beam fields, or they express the fields in terms of an infinite series of spherical multipole partial waves with specified coefficients [90].

To generate a Gaussian beam profile the laser beam has to be extended before it enters the microscope. A scheme of an optical trap is shown in figure 2.4. After the beam is expanded in most cases a beam steering unit follows. This component is not necessary but gives an extra degree of translational freedom. Afterwards, the beam is guided into the objective of the microscope. To position the beam a position detector can be used.

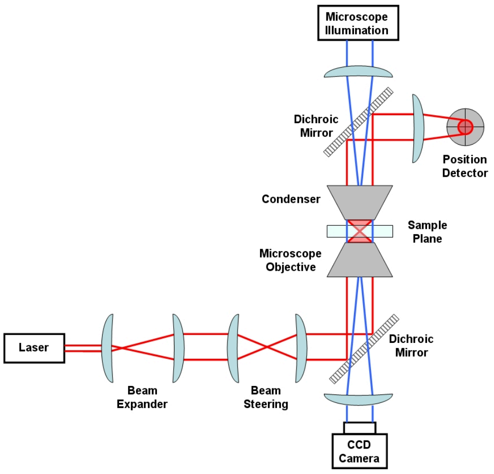

Fig. 2.4: Path of a laser beam into a microscope to create an optical trap. At first the laser is expanded, and then it might pass a beam steering unit to get an extra degree of translational freedom. Finally, the beam reaches the objective to get focused on the sample plane.

It is a good approximation to assume the particle underlies Hook's law $F_{trap} = k_{trap} \cdot x$. If k_{trap} is known it is possible to calculate the force exerted on an object by measuring it's distance from the center of the trap. Hook's law just holds for forces which are in x- and y-direction. Although, the trapped particle feels forces in z-direction as well, this force is much weaker than in x- or y-direction.

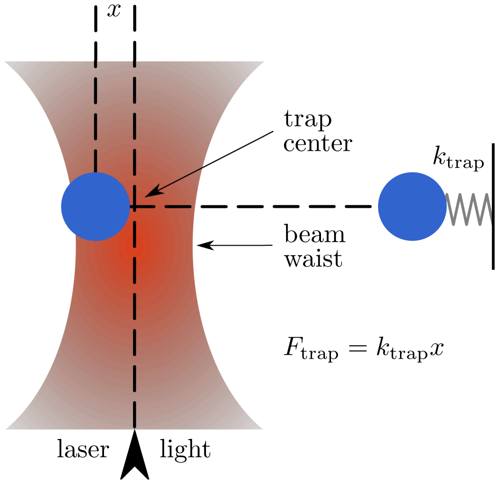

Fig. 2.5: Schematic of an optical trap. As long as the particle remains inside the laser beam it will be dragged towards the trap center. In the regime of low Reynolds numbers the trap force can be approximated by Hook's law.

Since the development of the optical trap, it has helped to understand basic processes in biology. In 1995 the force produced by a single molecule of RNA polymerase during transcription was measured by Yin and coworkers [91]. Furthermore, it was possible to measure the force-extension relationship of single DNA molecules, by using an optical trapping interferometer with feedback control [82]. By using a line of three optical traps Bronkhorst et al. showed that optical tweezers could also be used to deform a red blood cell and ‘fold’ the cell and observe the relaxation time [92]. Besides the biological applications, optical traps are used to assemble micro- and nano-devices, since they make contactless manipulation possible [93, 94].

2.6 Microfluidics

Future applications of bio-hybrid systems will probably not take place on a flat surface, but rather in a more complex two or even three dimensional environment. A way to build a two dimensional complex environment is the use of microfluidic techniques. Microfluidics covers the development, fabrication, and application of fluid handling micro-systems. The focus of research is on liquids in channels with a diameter of 1 μm up to 1 mm [95].

Microfluidic systems are normally used to reduce the amount of time and resources for chemical analysis and reactions, compared to standard methods. Due to the small scale of microfluidic channels other physical laws, than in our daily life play a key role, such that the system is mostly dominated by friction and not by inertial forces. This leads to a flow at Reynolds numbers much lower than one, so that the prevailing flow is laminar. Furthermore, changes in temperature, which are needed for some reactions, are much easier and quicker to accomplish, because of the smaller amount of fluid volume. The most common fields of use are chemistry, medicine, and biology. An example for the usage of microfluidics is the blood glucose level measurement of patients suffering from diabetics. A well-established technique to fabricate microfluidic structures is soft lithography. It grants the possibility to build structures with a size of 80 nm. In addition, this technique is very cost effective but easy to handle [96].

Methods

3

3.1 Cell Culture

D. discoideum AX2 wild-type and Lifeact-mRFP cells are cultivated in HL5 medium (Formedium, Norwich, England) at 22 °C on polystyrene Petri dishes (Primaria, Falcon, BD Becton Dickinson Europe, France), or shaken in suspension at 150 rpm. Before the chemotaxis experiments, the cells are washed and transferred into 25 mL shaking phosphate buffer solution (150 rpm), which consists of 14.6 mM KH_2PO_4 and 2 mM Na_2HPO_4 (Merck KGaA, Darmstadt, Germany). The resulting solution has a pH-value of 6.0. In this solution the cells are starved. After approximately three hours, the cells are washed again and afterwards mixed with a bead suspension (for details see section 3.6) to prepare them for the different experiments. For the uncaging experiments (for details see section 3.5) 10 μM BCMCM caged cAMP (BIOLOG Life Science Institute, Bremen, Germany) was added to the suspension. The cells had been left for 30 min inside the setups to attach before the experiment was conducted. For the experiments in HL5 medium cells are washed and the HL5 is exchanged with fresh one. Afterwards cells are filled together with the particle into a dish and left for 30 min before the experiment is started

3.2 Microfluidics

The microfluidic channel is manufactured from polydimethylsiloxane (PDMS) by soft lithography as introduced by Duffy et al. [97] for details see also [98]. Briefly, a silica wafer is coated with SU-8 2050 photo resist (micro resist technology GmbH, Berlin, Germany) in a vacuum spin coater (WS-400BX-6NPP/Lite, Laurell, North Wales, USA) to predefined height. After pre-baking, the coated wafer is illuminated with a UV lamp (Tamarack PRX 500, San Francisco, USA) through a photo mask (JD-Phototools, Hitchin, United Kingdom). After post-baking, the structure is developed in dev-600mr developer (micro resist technology GmbH, Berlin, Germany) until all non-illuminated photo resist is removed. After cleaning with 2-propanol and drying at room temperature, the wafer is ready to use for the micro-channel manufacturing process. For microfluidic chip fabrication, PDMS elastomer (Sylgard 184-Kit, Dow Corning, Wiesbaden, Germany) is mixed with curing agent in a $1:10$ ratio. The elastomer/curer mixture is poured onto the structured silicon wafer and the PDMS is polymerized at 75 °C in a laboratory oven (Thermofischer, Germany). Approximately five hours before the experiments start, the chip is cut with a scalpel out of the PDMS block on top of the wafer, inlet and outlet holes are punched into the PDMS with a syringe needle, and the PDMS block with the channel structure is plasma bonded to a glass cover slip in a vacuum plasma oven (Harrick, Ithaca, USA). A schematic sketch of this process is shown in figure 3.1. Buffer solution is filled into a micro-syringes (Harvard Apparatus, Holliston, USA), which is connected to the inlet structures in the PDMS microfluidic chip via PTFE tubing. The buffer solution is pumped through the microfluidic channel by a PHD Ultra micro-pump (Harvard Apparatus, Holliston, USA) to get rid of air bubbles inside the system. Directly before the experiment starts the pump is switched of and the mixture of cells, beads, and caged cAMP is injected into the channel. During the experiment no external buffer flow is added in order to avoid that the beads are flushed away.

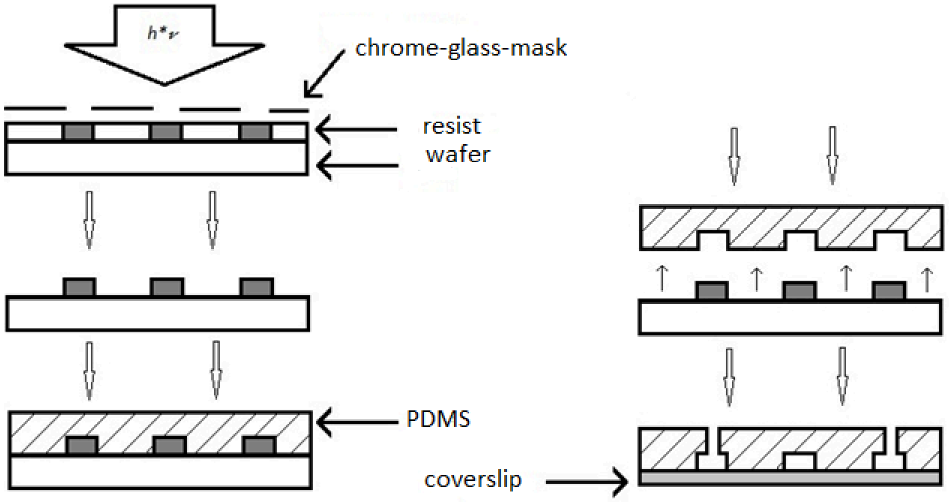

Fig. 3.1: A schematic sketch of the process of the soft lithography. First, the photo resist is illuminated through a chrome-glass-mask to harden the structure. Second, the not illuminated light is washed away and PDMS and curing agent is molded on top of the wafer. Third, the PDMS with the structure is cut out of the block and inlets are punched into the structure. Finally, the PDMS and a cover slip are placed into a plasma chamber to bond both together. Taken from: [99]

3.3 Imaging

To perform the experiments cells are filled into the micro-chamber or a dish and observed under a microscope for a couple of hours. Bright field microscopy is used in most cases. In addition, in some cases a confocal microscope is utilized to obtain fluorescent images. The time between the frames varies from 2 to 30 seconds depending on the type of experiment which is performed. Also four different microscope setups have been operated.

The single cell experiments, the gradient experiments in the ibidi chamber and the self-assembly experiments are observed under a *Olympus XI 71* microscope (Olympus Deutschland GmbH, Hamburg, GER) and recorded with an *ORCA-Flash 4.0* (Hamamatsu Photonics, Hamamatsu, JP). For the image acquisition the *HoKaWo* software, which has been delivered together with the camera, is applied to save the files. For the single cell experiments and the experiments in the ibidi chamber a 20x objective is used and an image is taken every 20 seconds. For the self-assembly experiments a 4x objective is utilized and an image is taken every 30 seconds.

To observe the cells during the uncaging experiments, a *Olympus XI 71* microscope is used together with a 20x objective and an *Olympus XM 10* camera (Olympus Deutschland GmbH, Hamburg, GER). Custom made software by Mathias Gerhardt is used to obtain and save the images as a windows bitmap (BMP) file. An image is taken every 30 seconds.

During the experiments with the optical trap the same setup as for the uncaging with a 40x objective is used. To obtain the images μManager (Open Imaging Inc., Mountain View, CA, USA) is used. An image is taken every 2 seconds. The files have been saved in .tif format.

For the experiments investigating the interaction of a single cell with a single particle a confocal microscope *Zeiss LSM 780* (Carl Zeiss AG, Oberkochen, GER) setup including a *ZEN* software package is used. An image is taken every 30 seconds.

3.4 Ibidi Gradient Chamber

In previous studies of *Dictyostelium* chemotaxis, linear cAMP gradients were generated by a microfluidic gradient mixer [34, 100]. Here the Ibidi μ slide 3D chamber is used instead, in order to avoid perturbations by the fluid flow. It contains two reservoirs which are connected by a small observation chamber with a width of 1 mm. For more detail of the chamber see figure 3.2. One reservoir contains the chemoattractand in case of the experiment 10 μmol cAMP. The other one contains a buffer. Inside the observation camber are cells and beads. Over 20 minutes a gradient of 10 nmol/μm is built up. This leads to a positive chemotactic effect on the cells [34].

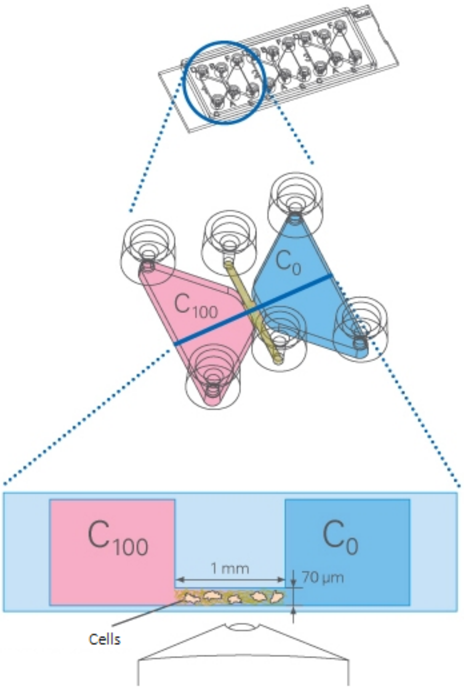

Fig. 3.2: Schematic structure of an Ibidi gradient chamber. Between the two reservoirs a static gradient forms. Cells follow the gradient throughout the observation area, where they can be imaged with the help of an microscope.

3.5 Photo-uncaging

For an efficient chemotactic guidance towards a single point it is important, that the chemoattractant is released only at that spot. For dish experiments with a single point source this is often accomplished by using a micro-pipette [101]. Cells move towards the pipette tip by following the chemoattractant diffusing out of that tip. By means of a micro-manipulator the tip can be moved in all directions inside the field of view. Nevertheless this approach is not feasible in a micro-fluidic chamber, since it is closed from all sides. To overcome this problem, cAMP is released with the support of an UV-Laser [102, 103]. Therefore 10 μmol cAMP coupled with [6, 7-Bis(carboxymethoxy)coumarin-4-yl]methyladenosine-3', 5'-cyclic monophosphate (BCMCM)(Biolog, Bremen, GER), the so called cage, is filled into the channel together with the cells. Because of the cage the cAMP cannot bind to the receptor and as a result is not detected by the cells.

To release the cAMP it has to be illuminated by a light of 330 - 370 nm wavelengths. The energy of the light breaks the bound between the cage and the cAMP molecule. Therefore cells are able to detect the cAMP without the BCMCM cage. In the present experiments a 355 nm laser (Genesis-355-150, Coherent, Santa Clara, CA, USA) with a power of 8 mW is used for uncaging. Using a UV laser grants the possibility

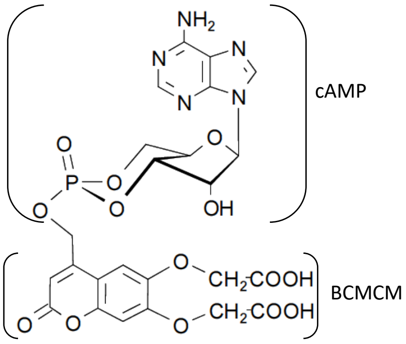

Fig. 3.3: Molecular structure of BCMCM-caged cAMP.

to release cAMP just on one single spot. In this way the cells can be guided to each point inside the chip. Unfortunately the setup does not give the opportunity to switch the laser on and off during the experiment time, leading to a permanent radiation over the whole observation time. Note that the light-induced release of cAMP can be also used to generate chemical gradients under flow conditions [104, 105]

3.6 Beads and Coating

For the micro cargo in the cell transport experiments, polystyrene beads of different sizes have been taken. The diameter of the beads varies from 4.5 to 75 μm. For the experiments coated and uncoated beads are used. Wheat germ agglutinin (WGA) is chosen for coating. Agar beads coated with WGA have been directly ordered (bioWorld, Dublin, OH, USA) and varied in diameter ranging from 10 to 25 μm. Furthermore, polystyrene beads (Polysciences Europe GmbH, Eppelheim, GER), (Microparticles GmbH, Berlin, GER) are used without coating, since no advantage in transport of the coated beads compared to the uncoated once is observed. Uncoated beads have been delivered in a mono-disperse particle suspension. Suspensions with a diameter of 4.5, 10, 15, 20, 45 and 75 μm are ordered from Ploysciences and 30, 45 and 60 μm are ordered from Microparticles.

3.7 Data Analysis

Prior to the analysis, the region of interest in the images are cropped manually with ImageJ (NIH, Bethesda, MD, USA) to reduce RAM capacity during processing, analysis time and possible tracking errors. The cropped images are analyzed with MatLab (version R2015a, MathWorks, Natick, MA, USA) together with the Image

Processing Toolbox. In a first step the images are converted to a binaries image. To do so the images the MatLab implemented function ’edge’ with the ’Canny’ method is used. The exact threshold level is chosen manually and varies 0.01 and 0.4. The lower the threshold the more sensitive the function is to fluctuations in intensity. While a low threshold value might detect natural intensity fluctuations in the images as well, a high threshold level could lead to missing fine structures. For the best result one has to find the best compromise between noise (low threshold level) and loosing information of the cell boundary (high threshold level). It could happen that the outline of an object is not fully detected by the ’edge’ function. To close possible gaps in the outline ’imclose’ is used. The function creates around every pixel with the value 1 a disk with a given radius. Every pixel inside this disk is set to 1, to fill up the missing parts in the outline. The next step to get an image with white cells on a black background is to fill the produced outline using ’imfill’. With the help of ’imfill’ every pixel inside a closed structure is set to 1. Since ’imclose’ increases the area of the cell it is necessary to erode the outline by the same size again. Therefore, the function ’imerode’ is used. This function reduces the outline by same size as it was increased before by setting the most outer pixels to 0. In figure 3.4 every step of the segmentation process is displayed. Afterwards, the center of mass is calculated and tracked throughout the images by a customized version of the tracking algorithm by Crocker and Grier [106]. The algorithm determines which particle in a given image corresponds to a particle in the preceding image by minimizing a cost function. In order to prevent skipping to a wrong particle in case of disappearance of the original one, a maximum distance and an area change of the particle between the frames is given. For more detailed information about the particle tracking algorithm see [106, 107].

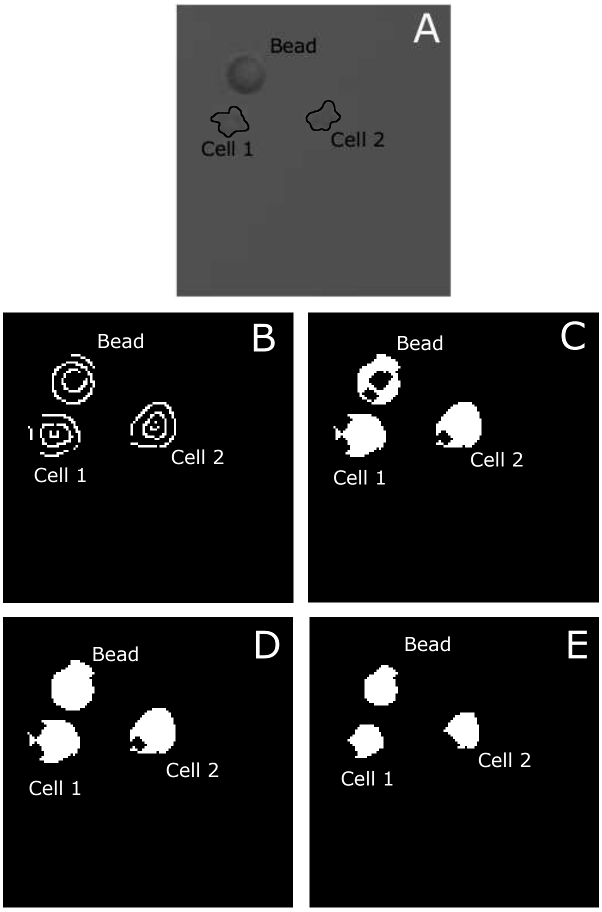

Fig. 3.4: An example of every step of the segmentation process. A is the raw image given into the algorithm. The outline of the cells and the particle in B is detected with an threshold level of 0.04. C shows the result of the 'imclose' function. In D the structures are filled, using 'imfill'. E shows the image which is used for tracking.

Results

4

This chapter presents the outcome of the experiments and shows the potentials and limits of *Dictyostelium discoideum* as a candidate organism for bio-hybrid systems. The chapter is structured as follows.

First, the movement statistics of single *Dictyostelium discoideum* cells were analyzed. In the next section polystyrene particles with different diameters are given to the cells. The interaction of cells with the particles was studied and the movement statistics of particles carried by a single cell evaluated. The third chapter gives an example for measuring forces generated by a single cell with the help of an optical tweezers and shows the limitations of this technique. In the last section the chemotactic behavior of the cells was exploited to carry particles towards specific locations inside the experimental setup.

4.1 Cell Movement Statistics

To get a better insight into the possibilities of amoeboid bio-hybrid systems it is important to understand the movement of the cells without any cargo. Therefore, 1143 single cell tracks have been recorded and analyzed with statistical tools. This work was done together with Dr. Andrey Cherstvy and published in [108]. Dr. Andrey Cherstvy performed the analysis of the scaling exponents and generalized diffusion coefficients shown in figure 4.5. He also fitted the reconstructed distribution to the step length distribution shown in figure 4.7 and calculated the collapse of the function shown in figure 4.8. Finally he fitted the Rayleigh and the generalized Gamma distribution to the distribution of instantaneous cell speeds presented in figure 4.9.

For the experiments cells were plated in HL5 medium on a dish under a *Olympus XI71* microscope. An image was taken every 20 seconds for six hours with an *ORCA-Flash 4.0* camera. Afterwards, the images were segmented with Matlab and cells were tracked. Examples of the tracking are shown in Figure 4.1. While, the minimum length of the tracks is 60 frames the length distribution varies up to 1000 frames, see Figure 4.2. There are several reasons for this spread of the track length. During the measurement cells can leave and enter the field of view. Furthermore, cells are able to divide during the experiment. This leads to an end of the track of the mother cell and a start of new tracks for the daughter cells. These things cannot be avoided and are natural causes for the end of a track or the beginning of a new one. Other reasons for the losing of a cell during the tracking could be the collision with another cell. In that case the algorithm cannot distinguish between the different cells and sees them as one. This leads to a losing of the both cells for the tracking and the start of new tracks when the cells move again apart from each other. A last possible reason for losing a cell during the track is a change in the contrast of the cell during movement. This could lead to a misdetection of the edge between cell and surrounding media. Especially the last point was tried to minimize during the tracking, by adjusting the threshold level.

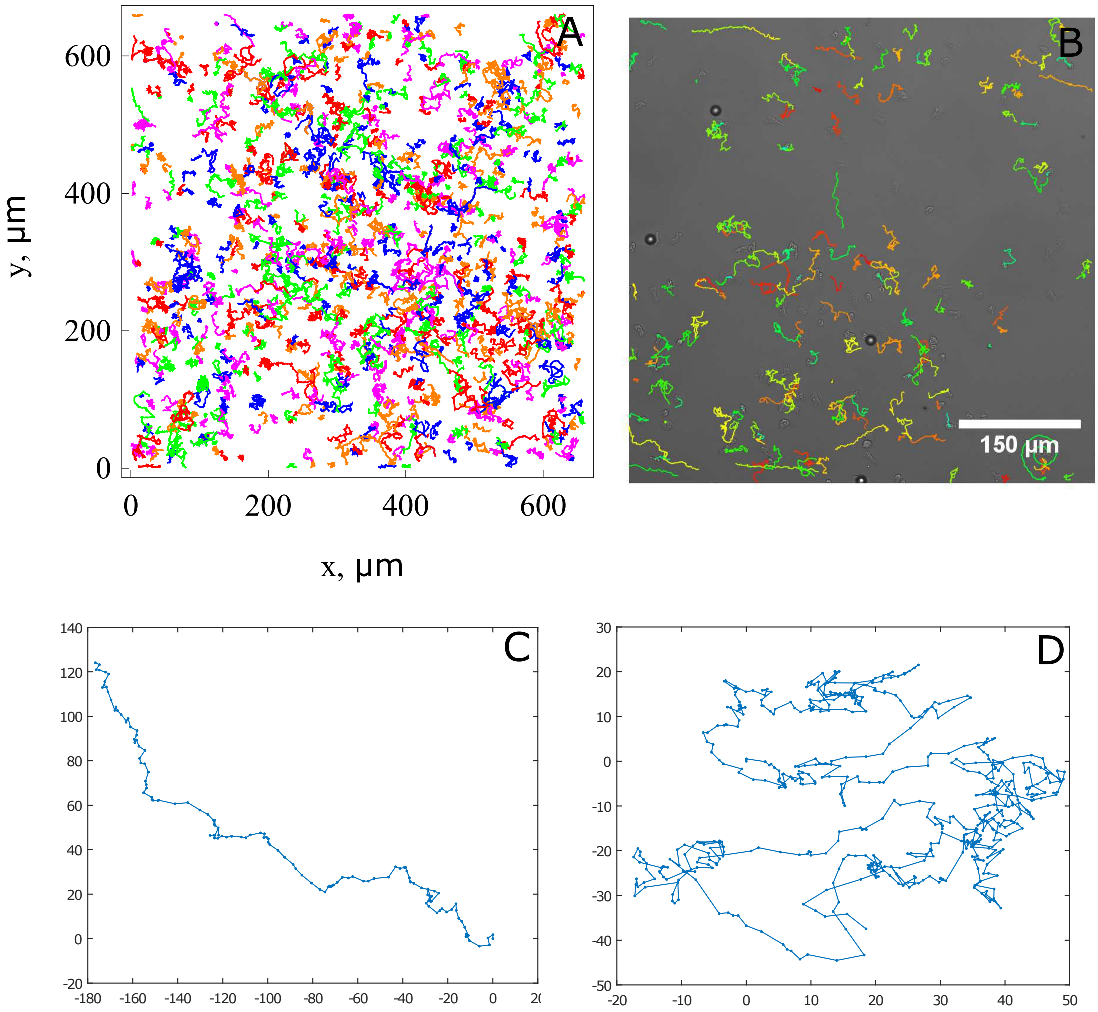

Fig. 4.1: Trajectories of the tracked cells. A shows the trajectories from 1069 tracks from five days of experiments. B shows cells on a microscopic image with the corresponding tracks. C and D show two different single cell tracks. Adapted from [108].

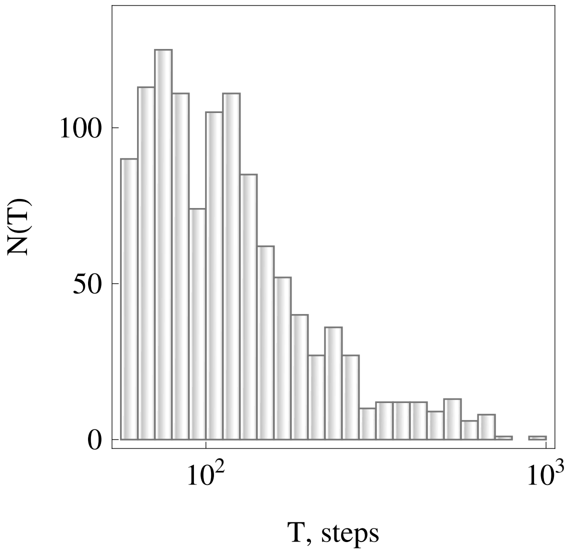

Fig. 4.2: Length distribution of recorded *Dictyostelium* trajectories, shown as counts on a linear–log scale (one step is $\delta t = 20$ s). Taken from [108].

To quantify the spreading of the cells based on the recorded tracks, the MSD curves of the cells were calculated in two different ways. First the ensemble average MSD was calculated as follows:

$$MSD(t) = \langle [x(t) - x(0)]^2 + [y(t) - y(0)]^2 \rangle \sim K_\alpha t^\alpha \tag{4.1}$$

Furthermore the time averaged MSD for each cell has been calculated,

$$\overline{\delta_i^2(\Delta)} = \frac{\int_0^{T-\Delta} \{[x_i(t+\Delta) - x_i(t)]^2 + [y_i(t+\Delta) - y_i(t)]^2\} dt}{T - \Delta} \simeq K_{\beta i} \Delta^{\beta i} \tag{4.2}$$

These time averaged MSDs have been averaged over all cells:

$$\langle \overline{\delta_t^2(\Delta)} \rangle = N^{-1} \sum_{i=1}^{N} \overline{\delta_i^2(\Delta)} \simeq \frac{\langle K_{\beta i} \Delta^{\beta i} \rangle}{T^{\alpha - 1}} \tag{4.3}$$

The results are shown in figure 4.3. The equations 4.1 and 4.3 were used for fitting. The resulting fitted lines in figure 4.3 gain an exponent of $\alpha = 1.28$ and $\beta = 1.37$. It is also visible in the figure, that the growth towards the end is much slower, than at the beginning. For the end phase the diffusion exponent is $\alpha \approx \beta \approx 0.3$. This leads to the question whether the decay is an aging effect or due to measurement artifacts. To test this tracks for three different groups of cells have been selected. The first group contains cells which tracks started within the first half hour of the experiment. The second group contains cells with tracks starting between 2 and 2.5 hours of observation. The last group contains cells starting between 4 and 4.5 hours of observation. The results for the ensemble averaged MSD is shown in figure 4.4. The diffusion exponent α changes from 1.20 to 1.22 to 1.10 over time. Although, the diffusion exponent is getting smaller for the last group, it is still in a super-diffusive regime. This indicates that there is only a minor aging influence.

Since cells are living organisms there are differences between them. This can be seen in the example trajectories in figure 4.1 and in the wide spread in the time averaged MSDs in figure 4.3. With the help of equation 4.2, asymptotes Dr. Cherstvy fitted the first $n_{fit}\{5, 15, 25\}$ points to quantify the corresponding β and K_β values. A strong anti-correlation was found, with the Pearson correlation coefficient for the $\{K_\beta, \beta\}$ sets being $\approx \{-0.56, -0.50, -0.51\}$ for $n_{fit}\{5, 15, 25\}$, shown in figure 4.5 together with the two-parameter fitted exponential slopes. This behavior indicates that cells either move very persistently with only low diffusivity or the cells have a high diffusivity but in a very random fashion, meaning less persistent.

$$K_\beta \sim \exp\left[-c_1\beta + c_2\right] \tag{4.4}$$

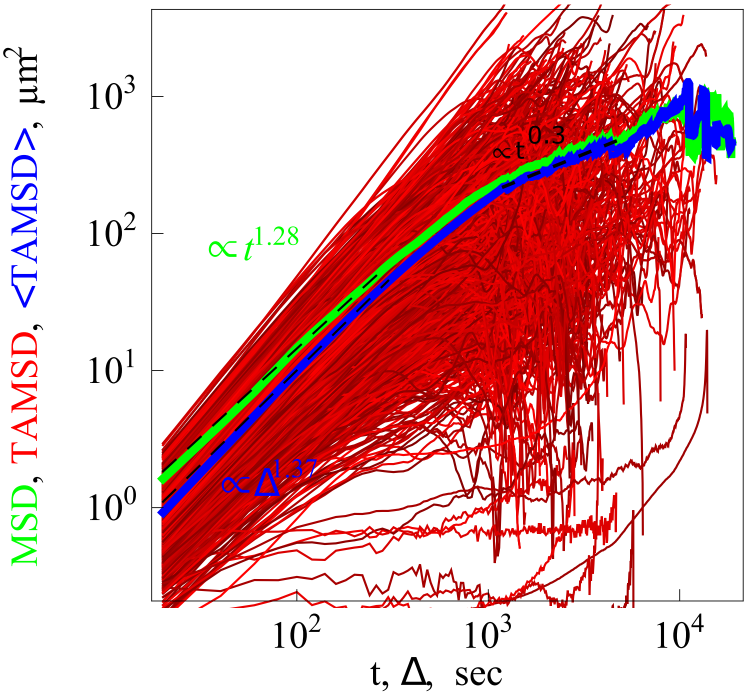

Fig. 4.3: Time averaged MSDs for 1143 single cells in red. The blue line displays the median of the 1143 time averaged MSDs while the green line displays the ensemble averaged MSD. Adapted from [108].

In a previous work it was stated, that *Dictyostelium* cell tracks varies between a diffusive search phase and a highly persistent phase of relocation [109]. To test this the mean persistence time was calculated out of the ensemble averaged MSD curve, following [110]. Therefore, the asymptote was fitted to the MSD curve. The intersection of the asymptote with the t-axis gives the value for the mean persistent

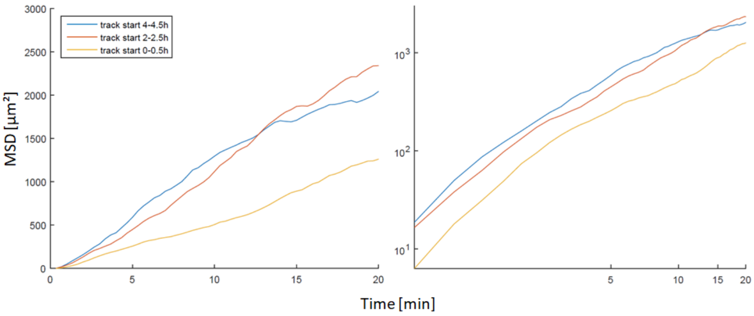

Fig. 4.4: Ensemble averaged MSD curves for cell tracks starting within the first half hour, between 2 and 2.5 hours and between 4 and 4.5 hours of experiment time.

time. This leaded to a mean persistence time of 2 minutes. As the persistence is low during the diffusive phase and high during the relocation this time was doubled to take that into account. To measure the persistence during this time the distance between both time points was divided by the length of the actual path the cell took to get there. The value will always be below 1. The more persistent a phase is the closer will the value get to 1.

The results of this measurement are shown in the histogram in figure 4.6 A. One can see a distribution between 0 and 1 with a maximum at 0.42. This result indicates that there are phases with a high persistent and also non-persistent phase. In figure 4.6 B the persistence over time for a random cell has been plotted. An alternating between more and less persistent phases is visible. To test whether there is an intrinsic switching time between those phases a mean correlation function for the cells was calculated. The function is plotted in figure 4.6 C. It shows a strong decay for the first 20 minutes followed by a slower decay. This indicates that there is no intrinsic switching time between persistent and non-persistent phases. To check whether this might change over time, the same analysis was done for cell tracks starting at the beginning, in the middle and at the end of the experiment. The results are shown in figure 4.6 D. The overall trend looks the same for all three curves, but the decay at the beginning seams to increase with time.

Besides the total movement of the cells over the whole observation time, the instantaneous movement from frame to frame is another interesting aspect of cell motility. To characterize this PDFs of *Dictyostelium* displacement have been examined with focus on the pronounced non-Gaussian features. The distributions of the displacement $p(\delta x)$ for all cells along the x coordinate with the time-shifts $\delta t = 20$, 60, 200, and 600 seconds are displayed in figure 4.7. The distributions along the y coordinate, $p(\delta y)$, shows a nearly identical appearance and can be seen in the appendix. To keep things simple, in the following only $p(\delta x)$ is considered. But the same analysis could be done for $p(\delta y)$. The shape of the $p(\delta x)$ show more pronounced cusps then

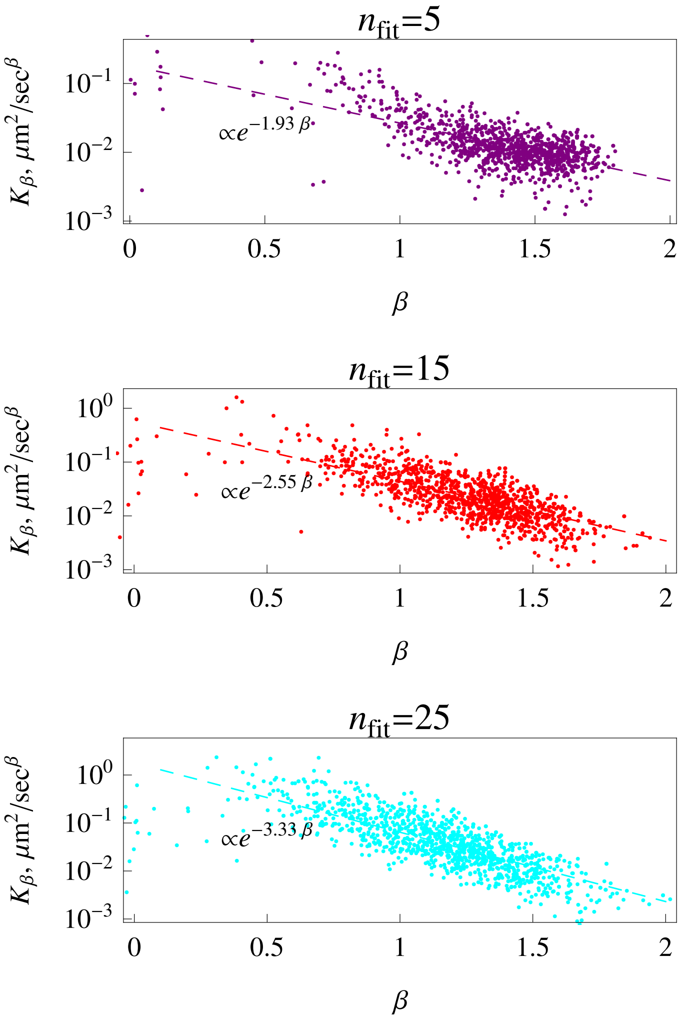

Fig. 4.5: Anti-correlation of scaling exponents and generalized diffusion coefficients for the data of Fig. 4.3. The best-fit asymptotes are the dashed lines. Results are shown for $n_{fit} = \{5, 15, 25\}$ initial fitting points of the $\overline{\delta_t^2(\Delta)}$. Done by Dr. Cherstvy. Taken from [108].

a standard Gaussian, while the decay of the tails is slower than Gaussian. For a closer analysis Dr. Cherstvy used Wolfram Mathematica to fit a reconstructed distribution $p(\delta x)$ with a two-parametric zero-mean compressed exponential or stretched Gaussian distribution,

$$p_{\delta,\sigma}(\delta x) \approx \frac{1}{2\sigma^2\delta^{1/\delta}\Gamma(1+1/\delta)} \exp\left[-\frac{1}{\delta}\left(\frac{|(\delta x)|}{\sigma}\right)^{\delta}\right] \tag{4.5}$$

In this equation σ displays the characteristic width of the distribution and $\Gamma(x)$ is the Gamma function. The notation δ for the exponent goes back to [111] and is not to be mistaken for $\overline{\delta^2(\Delta)}$ or space or time increments, δx or δt. The exponent δ

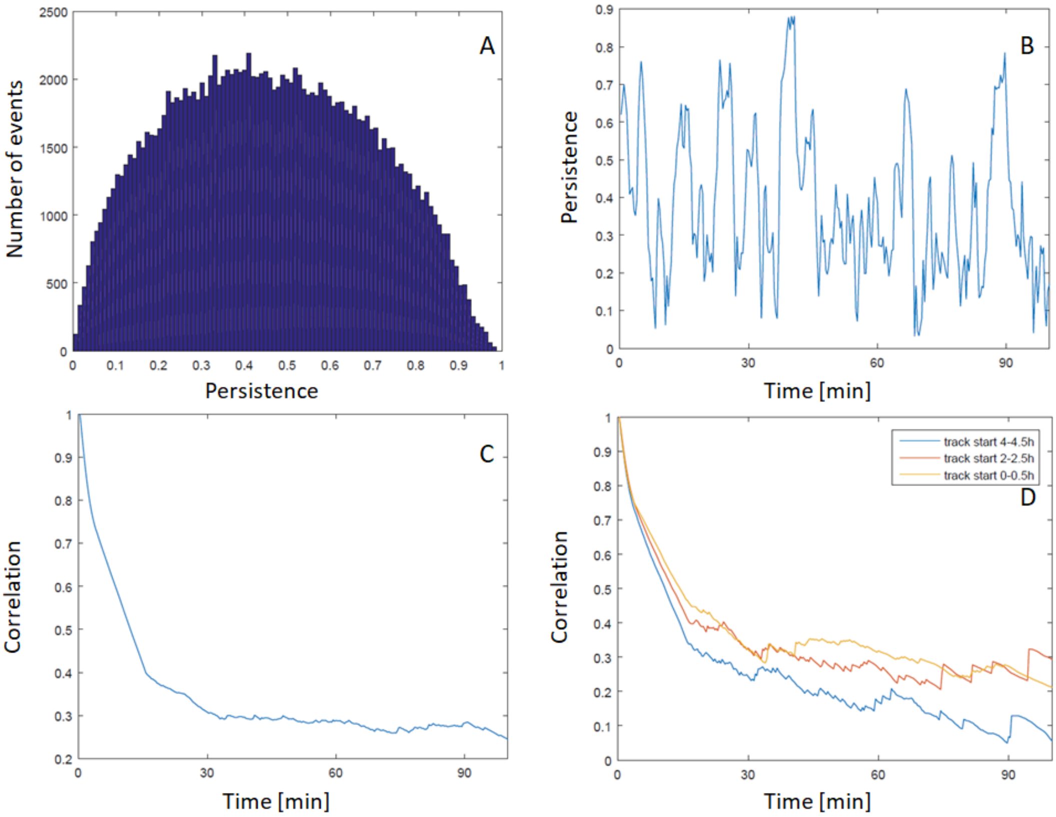

Fig. 4.6: Measure of persistence and intrinsic switching time between persistent and non-persistent phases. A) histogram of persistence distribution. B) persistence over time for a randomly chosen cell. C) mean correlation function of the cell persistence. D) mean correlation function of cell persistence for the three subsets.

quantifies the decay of $p(\delta x)$ away from the cups. Figure 4.7 shows that it is close to unity. As a result the exponential distribution is more Laplace-like than Gaussian. Furthermore, for an increase in δt there is a slightly decrease in δ. This feature indicates that the dynamics of the cells slows down in terms of the exponent $\langle\beta(\Delta)\rangle$ for longer lag time Δ. The averaged squared cell displacements along the x-achses, $(\delta x)^2$, scales with δt as follows:

$$\langle\overline{(\delta x)^2(\delta t)}\rangle = 2\int_0^\infty (\delta x)^2 p_{\delta,\sigma}(\delta x)d(\delta x) = \frac{\sigma^2(\delta t)\langle\delta\rangle^{2/\langle\delta\rangle}\Gamma(3/\langle\delta\rangle)}{\Gamma(1/\langle\delta\rangle)} \sim \sigma^2(\delta t) \qquad (4.6)$$

The weak dependence of the exponent δ on the time-shift was neglected, using the averaged value $\langle\delta\rangle$over all time steps δt for further analysis. As visible in figure 4.8 this approximation describes the displacement data well. The width of the distribution grows in a non-Fickian manner and was calculated form the best-fit parameters of the distribution functions of figure 4.7 and .1.

$$\sigma(\delta t) \sim (\delta t)^{0.615} \tag{4.7}$$

Therefore, the space increment δx shows a linear dependency on $(\delta t)^{0.615}$, leading to the rescaled space-time variable

$$z = (\delta x)/(\delta t)^{0.615} \approx (\delta x)/(\delta t)^{\alpha/2} \tag{4.8}$$

Finally this rescaled displacement distributions for different time-shifts collapse onto the universal master curve as shown in figure 4.8,

$$p_{\delta,\sigma(\delta t)}(\delta x) \sim \exp\left(-\left[(\delta x)/(\delta t)^{0.615}\right]^{\delta}\right) \tag{4.9}$$

The displacement divided by the time step is an approximation of the instantaneous speed of the cells,

$$v_i = \frac{\sqrt{(x_{i+1}-xi)^2+(y_{i+1}-y_i)^2}}{dt} \tag{4.10}$$

For an equilibrium system with an average squared particle speed of $\langle v^2 \rangle = 2\sigma_v^2 = 2k_b\frac{T_{eff}}{m}$ where T_{eff} is the effective temperature and m is the particle mass, a Maxwell-Boltzmann profile would be expected. This would correspond to the one-parameter Rayleigh-like distribution:

$$p_{Ray}(v) = \frac{v\exp\left[-v^2/(\delta 2\sigma_v^2)\right]}{\sigma_v^2} \tag{4.11}$$

As shown in figure 4.9 this function is not suited to describe the data. A much better agreement is achieved by a two-parameter Gamma distribution

$$p_{Gam}(v) = \frac{\gamma v^{\epsilon\gamma-1}\exp\left[-v^{\gamma}\right]}{\Gamma(\epsilon)} \tag{4.12}$$

The function shown in figure 4.9 is $p_{Gam}(v) \approx 0.90e^{-v0.96}v^{1.06} \sim ve^{-v}$. This means that the high-speed tail of the $p(v)$ distribution is approximately exponential.

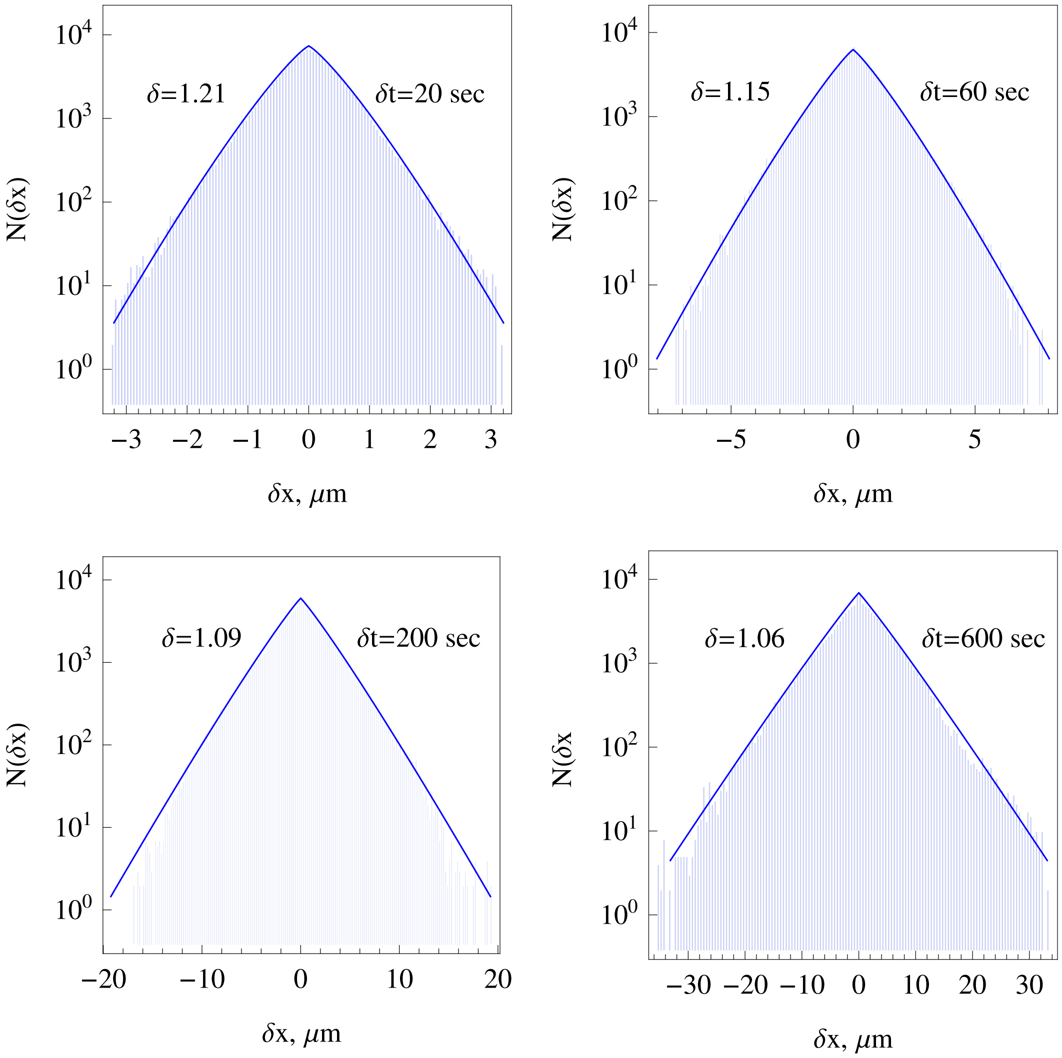

Fig. 4.7: Log–linear histograms of the number of cell displacements along the x direction for different time-shifts δt, as indicated in the plots. Different horizontal scales in the panels are to be noted. The asymptotes are the blue curves, with the values of the best-fit exponent δ provided in each panel. Taken from [108].

4.2 Random Particle Transport

As cells interact with the micro-objects, it is important to know how their moving behavior is influenced by the objects. Therefore cells have been placed in a dish together with particles of different sizes. Besides uncoated polystyrene particles, beads coated with wheat germ agglutinin and Cell-Tak has been used.

At first uncoated polystyrene particles of different sizes were placed in a 24-glass-bottom well-plate together with the cells in HL5 medium. For these experiments the LSM microscope was used with a frame time of 30 seconds. The aim was to investigate the influence of the particle size on the cell movement. Beads with a

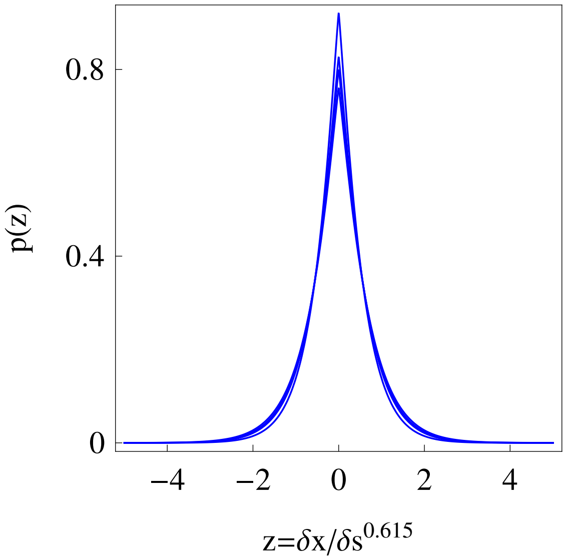

Fig. 4.8: Collapse of probability distributions over the rescaled variable z given by equation 4.8. The results are plotted for the time-shifts and mean scaling exponent $\langle\delta\rangle$ from the data set of figure 4.7. Done by Dr. Cherstvy. Taken from [108].

Tab. 4.1: Success of particle pick up after an overlap of the cell outline and the projected circumference of the cargo particle.

	Number of collisions	Number of successful pick up	success rate [%]
10 μm Beads	27	18	66.67
20 μm Beads	44	24	54.55
30 μm Beads	21	17	80.95
45 μm Beads	22	16	72.73
60 μm Beads	24	20	83.33
75 μm Beads	19	13	68.42

diameter of 10 μm, 20 μm, 30 μm, 45 μm, 60 μm and 75 μm were used during the experiments. Afterwards, the particles, carried by a single cell, were tracked and the MSDs and average velocities were calculated and compared with cells that did not carry any beads.

Since not every cell particle contact leads to a successful attachment of the particle, the first task was to calculate the rate of successful collisions. While details of the cell-particle contact are difficult to image, a success rate of collisions was quantified by analyzing events, where the outline of the cell overlapped with the projected circumference of the cargo particle. Particles with a diameter of 20 μm have with approximately 55% the lowest success rate while particles with a diameter of 60 μm have the highest success rate with approximately 83 %. The results are shown in detail in table 4.1. The result of a successful pick up is displayed in figure 4.10.

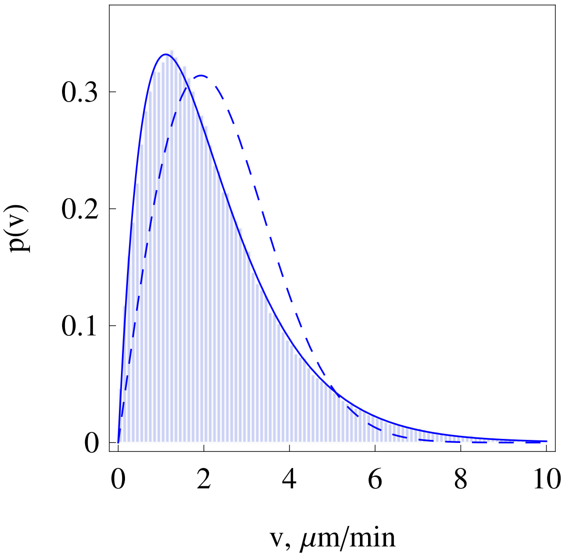

Fig. 4.9: Distribution of instantaneous cell speeds $p(v)$ and its fit by the Rayleigh (dashed curve) and generalised Gamma (solid curve) distributions. Done by Dr. Cherstvy. Taken from [108].

If a particle is successfully attached, it was tracked with the help of Matlab. Afterwards, the velocity for the particles have been calculated and averaged first over the single track and then over the particle size. Figure 4.11 shows the velocity distributions for the different settings. The results indicate three different velocity regimes. Particles with a diameter of 10 μm and 20 μm move with an average velocity of approximately 4 μm/min; cells without cargo and particles with a diameter of 75 μm move with an average velocity of approximately 6 μm/min; and particles with a diameter of 30 μm, 45 μm and 60 μm move with an average velocity of approximately 9 μm/min. For exact values see table 4.2. The velocity can be used to calculate the drag force of the cells via the Stokes equation.

$$F_R = 6\pi \cdot r \cdot \eta \cdot v \tag{4.13}$$

In this equation r gives the radius of the transported particle, η symbolizes the viscosity of the buffer and v is the velocity of the particle. The highest drag force is reached by particles with a size of 60 μm. The average drag force for such particles is 171.5 fN. While the maximum drag force is 360 fN. For all drag force values see table 4.2.

Besides the velocities the ensemble averaged MSDs have been calculated from the different tracks. Figure 4.12 shows the MSD for the different particle sizes and for cells without particles. The largest slopes in the MSD curves are reached by particles

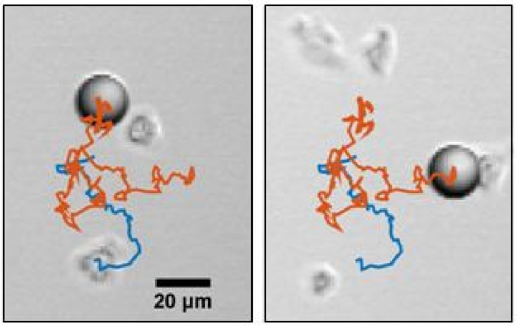

Fig. 4.10: A cell picks up a particle with a diameter of 20 μm and carries it around. The trajectory of the cell is shown in blue and the movement of the particle is displayed in red. The left image shows the first frame of the experiment while the right picture shows the last.

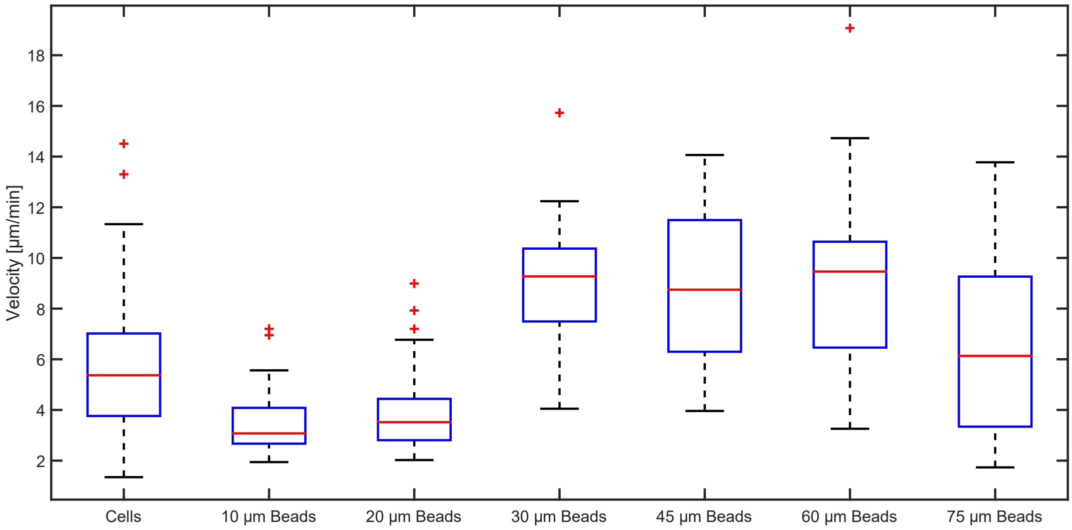

Fig. 4.11: Distributions of the mean speeds of beads with different sizes that are carried by single cells

with a diameter of 45 μm. This indicates the existence of an optimal cargo size for transport. For a normal diffusive process the relation $MSD = 2nD\tau$, with n is the number of dimensions and τ equals the time interval between the steps, helps to derive the diffusion coefficient for the cells and the cargo from the MSD curves. Therefore, the slope of the curves needs to be divided by 4. The results are shown in table 4.2.

As the results in the chapter 4.1 indicate the movement of the cells is not a normal diffusive process, but shows a super diffusive regime at early times. This can also be seen as a linear fit did not perfectly match the MSD curves. Therefore, the diffusion coefficient have been corrected by using only the beginning of the MSD curve for its' calculation instead of the whole curve. Furthermore the diffusion exponent α

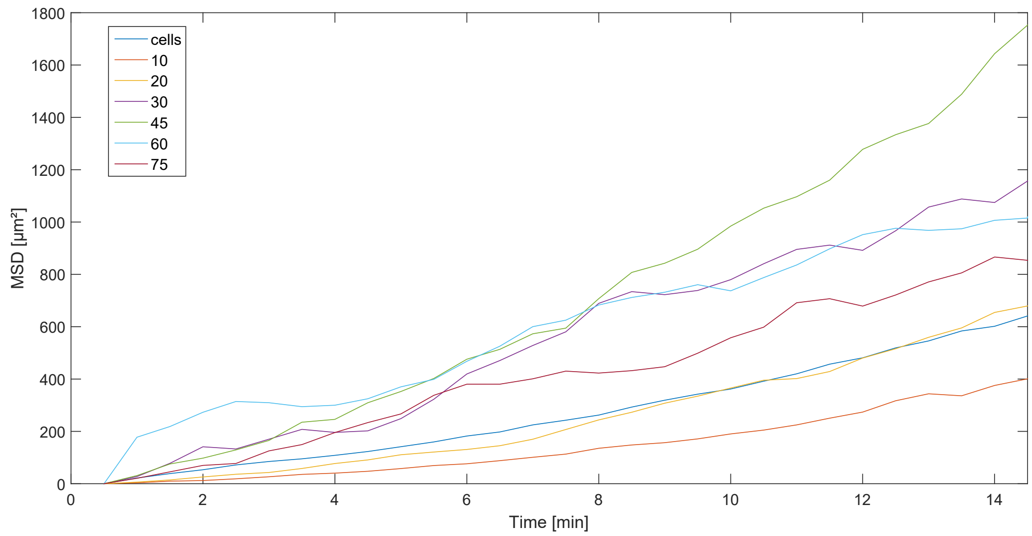

Fig. 4.12: Mean square displacement of cells and different bead sizes

was calculated using equation 4.1. In figure 4.13 the MSD curves are plotted on a logarithmic scale and the corresponding fit is shown in a dashed line. The results are shown in table 4.2 as well.

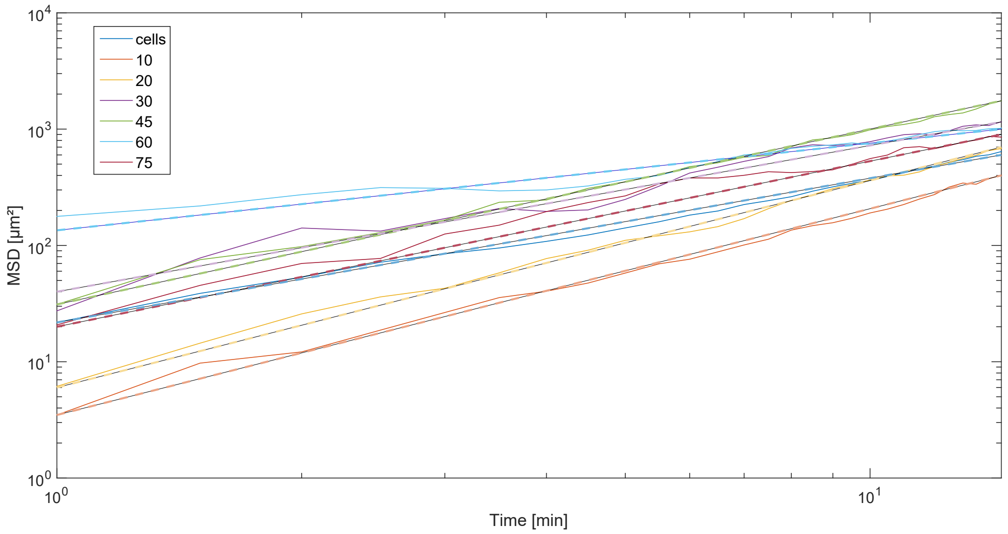

Fig. 4.13: Mean square displacement of cells and different bead sizes in a log-log plot. The dotted lines are fitted to the curves to calculate the diffusion exponent.

Tab. 4.2: Movement statistics for cells without cargo and for different cargo sizes carried by a single cell

	mean v [μm/min]	max. v [μm/min]	mean F [fN]	max F [fN]	D [μm^2/min]	D adjusted [μm^2/min]	diff exponent	♯ of tracks
Cells	5.6	14.5	-	-	4.83	4.41	1.25	313
10 μm Beads	3.5	7.2	17.6	45.6	2.69	1.18	1.71	44
20 μm Beads	4.0	9.0	25.1	56.5	4.72	2.10	1.71	62
30 μm Beads	9.1	15.7	85.8	148.0	9.68	7.8492	1.30	30
45 μm Beads	8.7	14.1	123.0	199.3	12.64	6.49	1.44	27
60 μm Beads	9.1	19.1	171.5	360.0	9.60	17.7	0.72	33
75 μm Beads	6.3	13.8	148.4	325.2	7.20	5.45	1.33	20

4.3 Optical trap

To quantify the potential of *Dictyostelium* as a transport system for micro-cargo, it is important to know how much force can be generated by a single cell. A first attempted has been done in chapter 4.2 by calculating the maximum drag force achieved during the particle transport.

The disadvantage of this method is the need to track the transport of particles with various different sizes to reach a maximum value achieved by a single cell. Furthermore, the velocity of a particle fluctuates strongly during the transport. Thus, only an average over the time step Δt is known. Another way is to apply a force directly to the transported particle. Therefore an optical trap was used.

4.3.1 Construction of the Optical Trap

To perform the experiment an optical trap has been build. For the trap a laser with a wavelength of 1064 nm was used (Coherent, Santa Clara, USA). The laser power can be increased in 0.5 W steps. Unfortunately, the objective is just capable to withstand laser powers up to 2.5W. This reduced the number of possible measurement point to five. To increase the number of measurement points a 50/50 beam splitter (BSW42-1064, Thorlabs, Newton, NJ, USA) was placed into the light path. The not needed part of the laser beam was send into a beam dump (BT610, Thorlabs, Newton, NJ, USA). After passing through the beam splitter the remaining laser beam is guided by mirrors (ME2-P02,Thorlabs, Newton, NJ, USA) towards the microscope. Directly before the laser enters the microscope it passes through two lenses (LA1540-ML and LA1560-ML,Thorlabs, Newton, NJ, USA). The lenses expand the beam to get a Gaussian beam profile after the laser passes the objective. This profile is needed to create an optical trap. A beam steering unit is not used in this setup, as the extra degree of translational freedom is not needed. The laser beam is focused with a Zeiss 40x oli objective (EC Plan-Neofluar 40x/0.75 M27, Zeiss, Jena, Germany) in the field of view. The microscope had no port to insert a position detector. Therefore, it was not possible to integrate a position detector into the setup. The positioning of the laser was achieved by trapping multiple particles, as shown in figure 4.14. These particles were arranged in a line in z-direction to be sure that the beam passes orthogonal towards the sample plane through the probe. An image of the setup can be seen in figure 4.15 and as a scheme in figure 4.16.

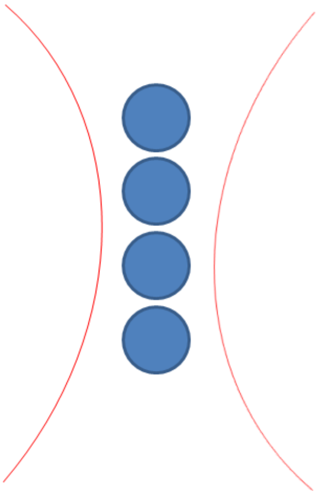

Fig. 4.14: Scheme of how to align and position the laser with the help of multiple traped objects.

4.3.2 Determining Properties of the Optical Trap

At first the properties of the trap have been determined. Therefore, a micro-particle was trapped and moved through the liquid with a fixed velocity. The Force applied to the particle was calculated over the Stokes-equation: $F = 6\pi r\eta v$. When moving the trapped particle the Stokes force is pushing the particle out of the trapping potential. When the force is high enough the particle overcome the potential and snaps out of the trap. To measure the maximum of the force generated by trap, the velocity of the particle was increased stepwise. The maximum was reached when the laser was just able to keep the particle trapped. Any further increase of the velocity would lead to losing the particle. The correlation between the maximum force generated by the trap and the laser power is shown in figure 4.17. It is an exponential dependence with an exponent of 1.32. The maximum force reached with this setup is 630 pN. To measure the force particles with a diameter of 10 μm were used. The force of the optical trap depends on the particle size. It will increase for smaller particles and decrease for bigger once. The 10 μm particles had been used as they were able to trap also with low laser powers and have also a relevant size for the random particle transport experiments presented in section 4.2.

The displacement of the particle out of the center of the trap was measured with the help of the Matlab tracking algorithm. The displacement of the particle from the trap center and the known force can be used to calculate the k value with the help of Hooke's law for the different laser intensities. An example of such a curve is given in figure 4.18. It is visible that the particle displacement for high velocities did not follow a linear trend as it should be. One reason could be that Hooke's law just holds

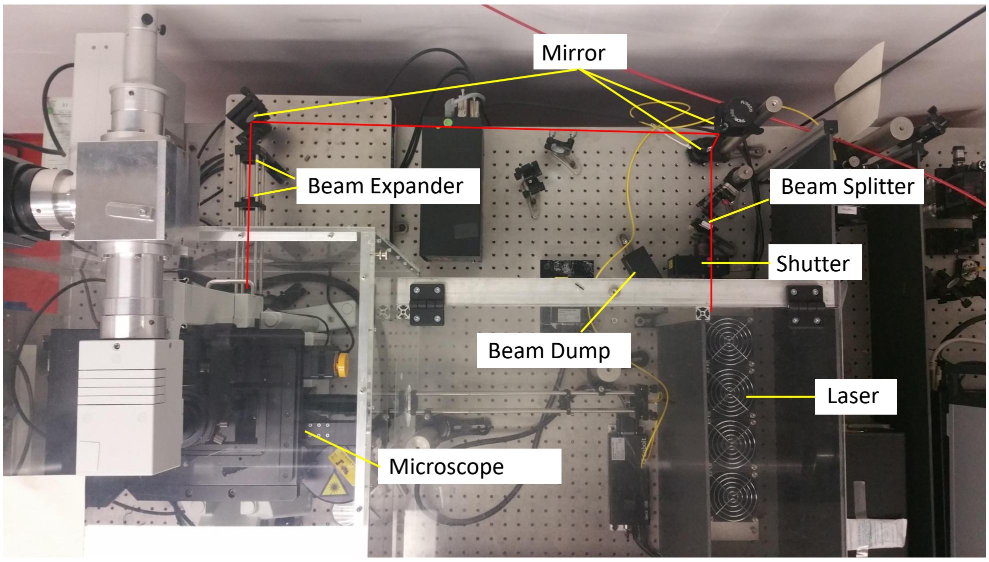

Fig. 4.15: Setup of the optical trap. At first, the beam passes a 50/50 beam splitter. Afterwards, it is guided with the help of mirrors towards the microscope. Before the beam enters into the microscope it is widen with the help of a beam expander.

for small displacements out of the trap center. It is also possible, that the speed of the stage gets less accurate for higher values. Although, the speed was checked to be correct for slow values with the help of an object-micrometer. There could be an error when the stage moves faster.

4.3.3 Measuring forces with the Optical Trap

For the measurement a particle trapped by the laser beam was brought in contact with a cell. As long as the displacement is small, the force applied to the bead is linear with respect to its displacement from the center of the trap. In this way it is possible to calculate the force applied with the help of Hooke's law $F_{trap} = k_{trap} \cdot x$ when the cell pulls on the particle.

But there are also some problems with this technique. On the one hand the IR laser used for the trap is heading up the buffer solution the cells are suspended in and thus it is harmful for the cells. As a result cells might die during the experiments with high laser powers, consequently with strong forces generated by the optical trap. An evidence for this is that the cells start to round up when they are radiated by higher laser powers. Another problem is the way the cell applies the force to the

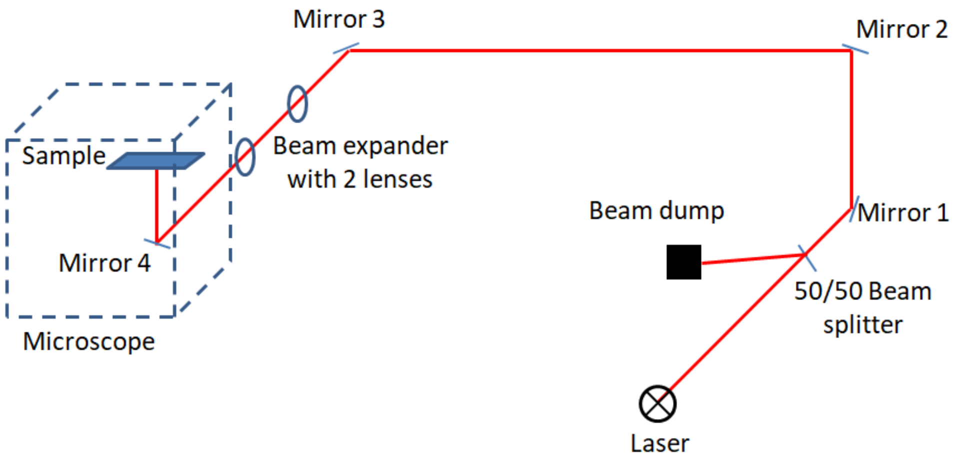

Fig. 4.16: A scheme of the optical trap setup. With the help of the mirrors 1 to 3 the laser beam can adjusted. Mirror 4 is inside the microskope and thus not moveable.

bead. To calculate the force acting on a particle it has to be applied orthogonal to the laser beam. Any force applied parallel to the beam cannot be calculated in a proper way, as the force-field in z direction is not known.

It was possible to apply forces up to 330 pN with a laser intensity of 3W, as shown in figure 4.17. Up to this intensity cells have been able to overcome the maximum trap force. In figure 4.19 it is visible that the cell is able to pull the bead out of the trap with a laser power of 3W. Although, it was possible to use higher laser powers, 3W did already harm the cells. In figure 4.20 it is visible that cells begin to round up and eventually die when exposed to the laser for a longer time period.

At laser powers below 1.5 W cells manage to get the particle out of the trap in all cases. Although, cells did not start to round up when the power of the laser increases up to 2 W, it seems, that this already starts to harm the cells, as they begin to crawl away from the laser beam.

4.4 Guided Particle Transport

Dictyostelium cells are able to sense gradients of the chemical messenger cAMP. The cells follow a cAMP gradient towards the higher concentration. They are able to sense shallow signals near the noise level as well as steep gradients, even in the presence of high offset concentrations. This behavior can be used to guide the transport of micro-beads and to assemble them. There are two possible approaches for the assembly of micro-particles. Cells can generate their own cAMP gradient

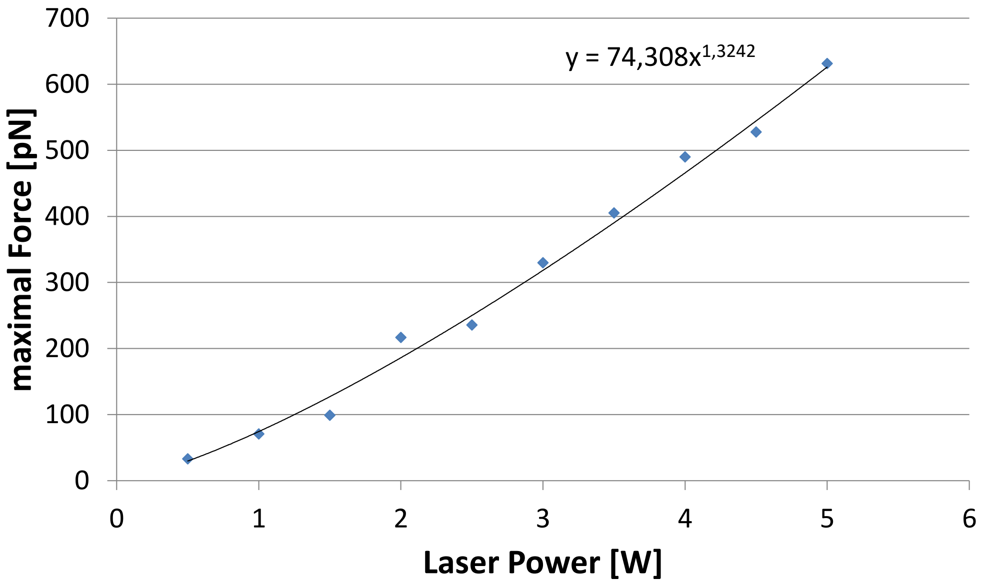

Fig. 4.17: Correlation between the laser power and the maximal force generated by the optical trap. The trapped particle had a diameter of 10 μm.

or an external cAMP source is given to guide the cells to a desired position and assemble the objects at that spot.

4.4.1 Selforganized assembly

During the development process *Dictyostelium* aggregates by secreting and following cAMP. This natural process can be exploited to assemble micro-objects. To demonstrate this, cells and particles with a diameter of 20 μm are distributed randomly on a dish in phosphate buffer, see figure 4.21 top right and bottom right. Over the time the cells start to aggregate. On their way they eventually pick up beads and carry them towards the aggregation center as well. This leads to the formation of small localized particle clusters (figure 4.21 middle top). As the development goes on, different clusters merge into a big final cluster. This process leads to a change from a homogeneous particle distribution to a heterogeneous one, see figure 4.21 top left and bottom left. The aggregation process was quantified by measuring the the distance from each particle to all other particles in the field of view. In figure 4.21 bottom the transformation from an initial distribution with a pronounced peak into a bimodal one can be seen.

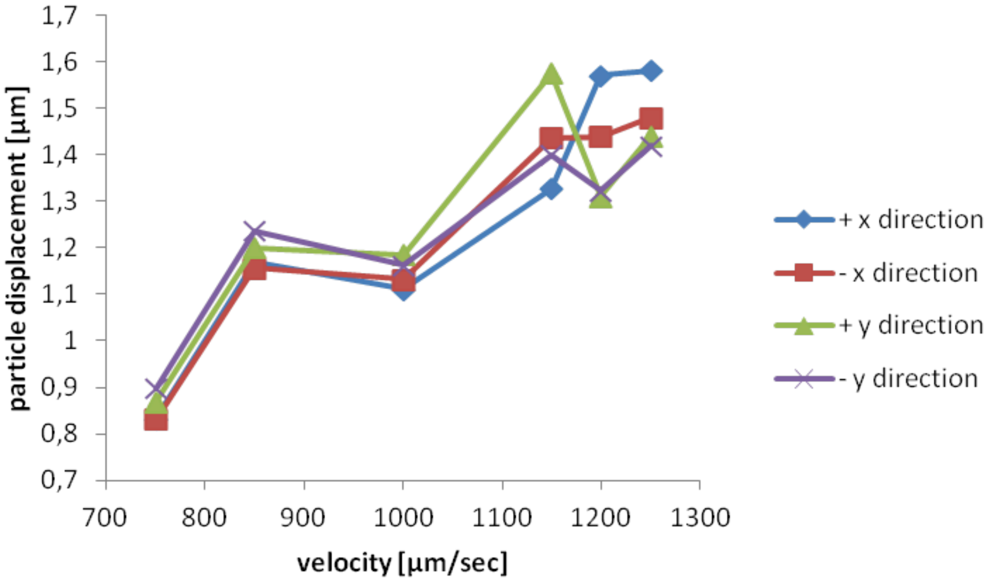

Fig. 4.18: Example curve of the optical trap to determine the trap properties for a laser power of 2.5 W. The calculated k value is $0.08 \pm 0.02\ \frac{kg}{s^2}$ at a maximum reachable force of 236 pN

4.4.2 Guidance by external cues

To guide the transport of particles towards a specific position an external cue is necessary. In this study a chemotactic gradient was used to guide the transporting cells. A static cAMP gradient was established with the help of a Ibidi μ slide 3D chamber. To generate a more flexible cAMP source, BCMCM caged cAMP was uncaged with the help of a UV laser. For more details see chapter 3.4 and 3.5.

Inside the Ibidi chamber a static cAMP gradient is formed, by filling one reservoir with 10 μM cAMP solution while the other one is filled with buffer. This leads to the formation of a linear gradient within the narrow connecting region between the two reservoirs, see figure 3.2. Starvation developed *Dictyostelium* cells were mixed with wheat germ agglutinin coated agar particles. The particle size varied between 20μm and 50 μm in diameter. Cells followed the gradient towards the higher cAMP concentration. On their way they eventually picked up a particle and carried it along. It is also possible that cells lose a particle while moving. Following cells might step in as new transporter. This process leads to a net particle flow up the gradient. In figure 4.22 the trajectory of a particle through the observation area is displayed. Furthermore, it is possible for two or more cells to transport an object together along their way to the higher cAMP concentration.

The stationary linear gradient in a diffusion chamber is easy to create but comes with several limitations. It is for example difficult to change the steepness of the

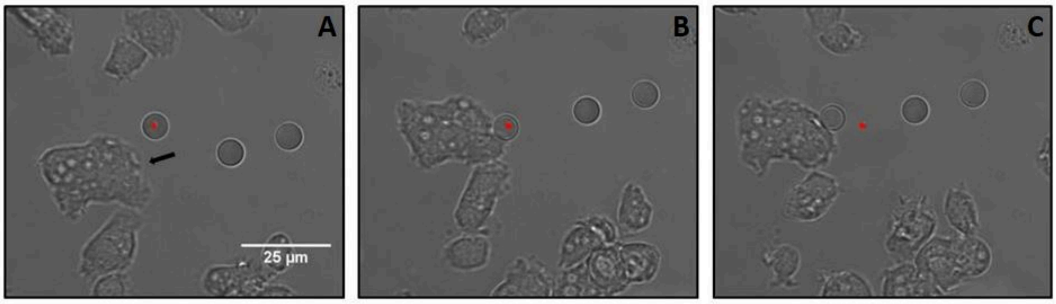

Fig. 4.19: A particle with 10 μm in diameter is brought in contact with a cell (A). The cell starts to pull on the particle (B). The cell overcomes the trap force and pulls the particle out of the trap (C). The red dot in the images indicates the position of the laser. The black arrow in the left frame highlights the cell the particle is attached to.

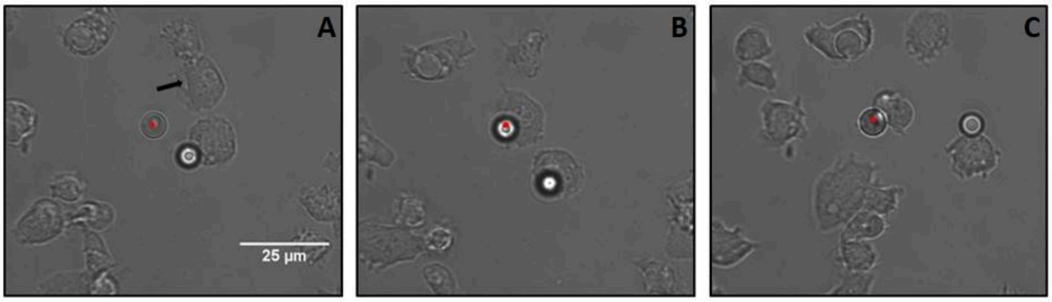

Fig. 4.20: A particle with 10 μm in diameter is brought in contact with a cell (left image). The cell starts to pull on the particle (middle image). The laser harms the cell so it starts to round up end eventually dies (right image). The red dot in the images indicates the position of the laser. The black arrow in the left frame highlights the cell the particle is attached to.

gradient. Also the direction cannot be changed easily. Another disadvantage is that the maximal distance for object transport is limited by the width of the diffusion chamber and by the properties of the chemoattractant receptors which might be saturated, if cells move in a continuously increasing gradient.

A more sophisticated way to guide the cells, that overcome some of these limitations, is the use of the photo uncaging technique. The chemoattractant is caged by a BCMCM-residue attached to the phosphate groupe of the cAMP. Because of the cage, cells are not able to detect the cAMP, as it do not fit into the receptor binding pocked anymore. A UV-laser is able to break the bond between BCMCM and cAMP so it fits again into the receptor binding pocked of the cells. Due to continued radiation with UV-light at a specific point, a radial gradient forms around the laser spot by diffusion. While the experiment is conducted, this chemoattractant point source can be flexibly repositioned allowing to access closed structures of complex geometry.

To demonstrate this approach, cells and WGA coated agar beads were suspended in 10 μM BCMCM-caged cAMP containing buffer and placed together in a glass-bottom

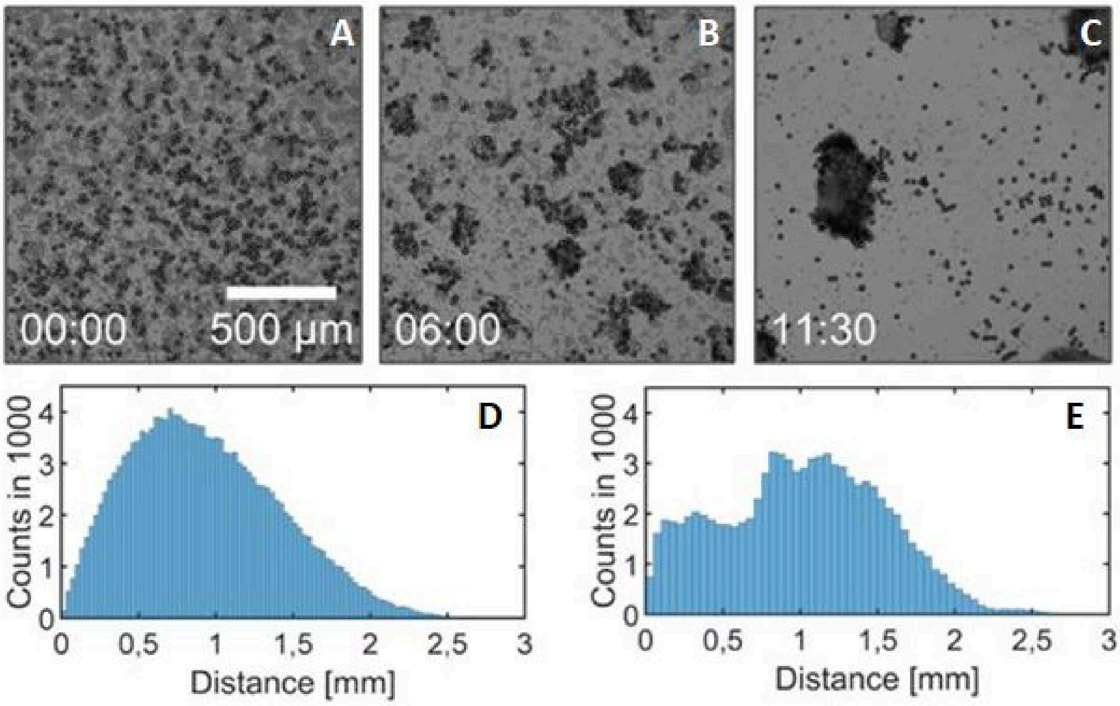

Fig. 4.21: The top shows the spontaneous aggregation process of the cells leading to a assembly of micro-objects. A is the first frame of the measurement. In B already small particle clusters are visible. C is the last frame of the measurement showing big particle aggregates. The bottom shows the corresponding histograms for first and the last frame. D is the corresponding histogram to image A, while E corresponds to image C.

Petri-dish. A laser with a wavelength of 366 nm was used to break the bond between the BCMCM and the cAMP. As a result, cells crawl towards the laser while dragging particles along, leading to a particle assembly around the laser spot. In figure 4.23, an uncaging experiment in a dish is shown. The laser breaks the bond between BCMCM and cAMP, leading to a radial cAMP gradient around the laser spot. Cells follow the cAMP signal and carry particles along. After three and a half hours an accumulation of WGA coated agar particles around the laser spot can be observed.

With help of this tool it is also possible to guide cells through a more complex structure like a channel system. Cells and polystyrene beads with a size of 4.5 μm were incubated together in phosphate buffer containing 10 μM BCMCM-caged cAMP. This suspension was given into a microfluidic channel with narrow dead-end side branches. A laser spot positioned in the side channel created a cAMP gradient along the branch and in the main channel. Surrounding cells sensed the cAMP, which diffused out of the channel and followed the gradient into the side branch. On their way, cells pick up one or more 4.5 μm beads and move the cargo with them into the branch. This is shown in Fig. 4.24. While cells are able to carry just a single bead when the size exceeds 10 μm, it is possible for them to carry 6 ± 2 4.5 μm particles.

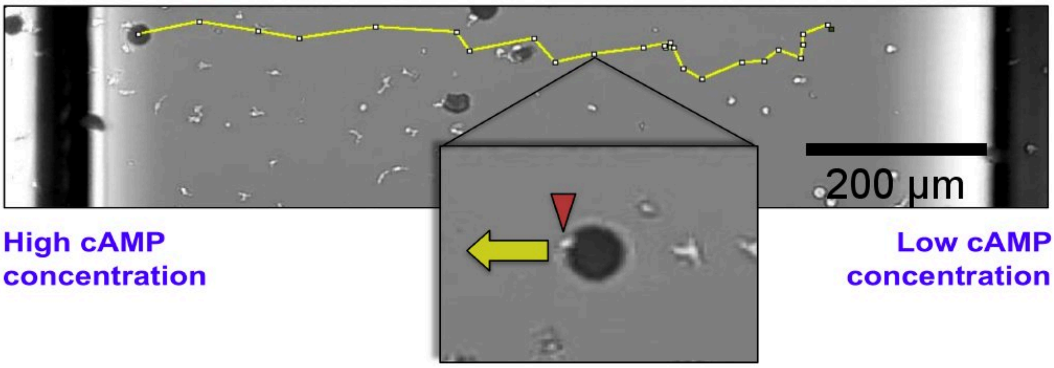

Fig. 4.22: Particle transport upwards a linear cAMP gradient. While *Dictyostelium* follows the cAMP gradient, cells may eventually pick up a bead and carry it along. The track of a bead is shown in yellow. The inset shows that the particle is only carried by a single cell.

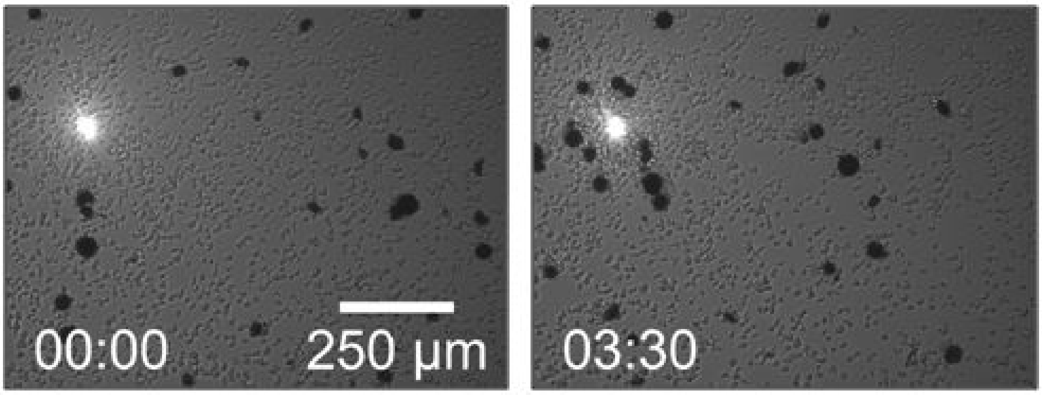

Fig. 4.23: Particle transport towards a laser spot due to photo ungaing of cAMP. After three and a half hour of observation cells and particles are close to the laser spot.

Thus the cells are able to transport particles rapidly through a complex environment, which would otherwise require laborious operations, like the one by one movement of individual particles with the help of optical tweezers.

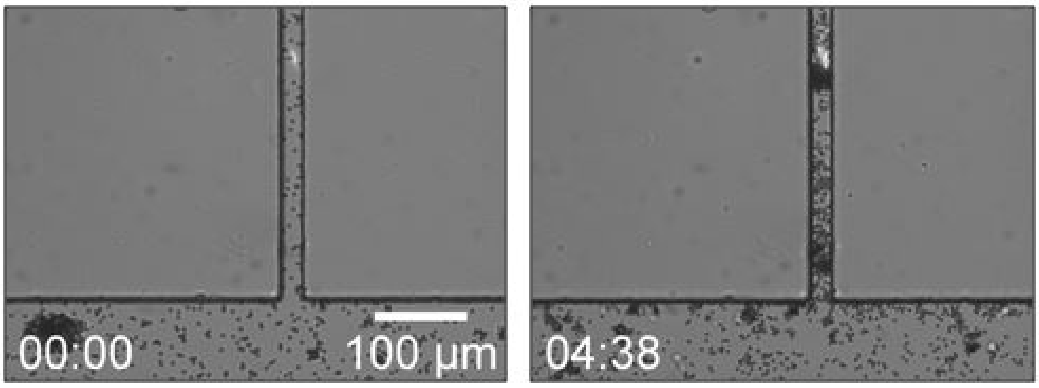

Fig. 4.24: Particle transport into a dead end channel structure due to photo ungaing of cAMP. Uncaged cAMP diffuses out of the side channel to attract the cells. On the way towards the high cAMP concentration, cells pick up small particles and carry them along.

Discussion

5

5.1 Cell Movement Statistics

Dictyostelium cells show, like all living organisms, differences in age, inherent variations in size and different propulsive characteristics throughout the population. This results in variations of the single cell movement patterns. As a consequence, the time averaged MSD show strong fluctuations. Similar variations of time averaged MSD curves can be observed in non-ergodic anomalous diffusion processes which can occur due to heterogeneous conditions across the system [112]. The ensemble averaged MSD and the mean of the time averaged MSD are quite close, but the amplitudes and scaling exponents do not match perfectly. This mismatch indicates weak ergodicity breaking [112]. Although the discrepancy between the curves is quite small it can be decreased further with more and longer tracks. The MSD curves increase slower and slower over time. The growth of the MSD, changes from $\alpha = 1.28$ and $\beta = 1.37$ to $\alpha \approx \beta \approx 0.3$. This is often associated with confinement or ageing in subdiffusion [112]. When the diffusion exponent of cell sets starting at the beginning, the middle and the end of the observation time, the decay of the exponent is much smaller. The effect of the strong decay of the exponent of the MSD of all tracks could be caused by the intrinsic limitations of the data acquisition. For example it is more likely for a fast moving cell to enter and leave the observation area than for a slowly moving one. This leads to shorter tracks for fast moving cells, as they start later or end earlier than the ones of slow moving cells. The outcome is a possible bias towards slower moving cells for long trajectories, resulting in an overall smaller magnitude for cell displacement. A similar reduction of the local scaling exponent has been detected for spreading protozoa [113].

The anticorrelation of the scaling exponent β versus the generalised diffusion coefficient K_β as shown in figure 4.5 also indicates that persistently moving cells show a smaller diffusivity. So far none of the standard anomalous diffusion processes [112] explains this type of anti-correlation. The viscoelastic diffusion of tracers in polymeric hydrogels, for example, shows a positive β versus K_β correlation [114]. A possible explanation for this behavior could be that some cells use the available energy to perform macropinocytosis, which could act like random motility, while other cells move more pseudopod driven,which leads to a more persistent type of movement. This could be a survival strategy [109, 115]. Some cells stay in one place with high nutrition to keep the specie alive, while others move away to spread over a wider area. Previous experiments indicated an anticorrelation between cell speed and the turn rate of the cells [50]. This is in contrast to the findings presented here, as fast moving persistent cells would achieve a greater diffusivity than slowly moving reorientating cells. Also Ref. [116] indicates that persistent and diffusivity is correlated. Nevertheless, the results indicate that cells alter between a random moving phase and a phase which is more persistence as reported by [109]. The findings in figure 4.6 seem to support this. But there is no intrinsic switch between both states. This means that each cell changes the walking pattern differently.

To describe the distribution of the instantaneous cell speeds in figure 4.9, the Gamma function with equation 4.12 was used. This had been done before to describe the instantaneous cell speed distribution of the spreading dynamics of protozoa cells [113]. The nearly exponential tails of the speed distribution can be compared with figure 4F in reference [117], measured in the *Dictyostelium* AX4 strain. Furthermore it can be compared to the mean velocity over a 15 minute interval for *Dictyostelium discoideum* cells in Ref. [118].

For the best fit exponent δ of the histogramms in figure 4.7 the decrease for bigger step shifts δs is with respect to the MSD data not surprising, as dynamics slow down for long lag times. The collapse onto the universal master curve has been detected recently [119]. In short, we conclude that *Dictyostelium* diffuses anomalously and shows a non-Gaussian displacement distribution.

5.2 Random Particle Transport

The results of table 4.1 of chapter 4.2 indicate that not all contacts of a cell with a particle lead to the formation of a bio-hybrid system. Nevertheless, the probability that a cell starts to transport a micro-bead after contact is higher than 50% for all tested particle sizes. There are two possible reasons for the cell to stay in contact with a micro-particle. The first possibility is that the cell tries to phagocyte the bead. This is probably the main reason for the 10 μm beads to stay attached to the cells. The other reason for the cells to stay in contact could be the fact that *Dictyostelium* likes to be in a confined environment and maximizes the surface area in contact to the surrounding [120]. This is especially the case for the bigger particle sizes of 30 μm and above. The reason why the rate of successful attachments is minimal for the 20μm bead could be that they do not suit one of the requirements. Big cells may still try to phagocyte the particles, but small cells still get a reasonable amount of confinement to stay in contact with the particle. For the majority of cells the particles are to big for phagocytosis and not big enough to grant a suitable area of confinement, making it less favorable for cells to stay in contact with the particle. Furthermore, the values given in table 4.1 represent a lower bound for the rate of successful contact. Since the microscope is just able to give a 2D projection of a 3D process, the overlap of the cell outline and the projected circumference of the cargo particle does not necessarily lead to a contact of both. In particular for large particles this mismatch between overlap and contact could gain more and more influence on the results.

The effects of phagocytosis and confinement are also important to explain the other results of the random particle transport. The mean velocity of the particles can be roughly divided into three regimes. The first regime with a velocity of approximately 4 μm/min contains the particles with 10 μm and 20 μm in diameter. This regime is slower than cells without cargo. Since the particle sizes are small, cells try to phagocyte them. The process of phagocytosis is slowing the cells down, as the cytoskeletal activity needed for the formation of pseudopods is now used to engulf particles. Furthermore, it was observed that Ras null cells, which are impaired in phagocytosis and fluid phase endocytosis moving faster than wild typ cells under growth conditions, but their speed becomes more wild-type-like during starvation [121]. This effect is stronger for 10 μm beads, since small cells do not try to engulf a 20 μm particle. The second regime has an approximate velocity of 9 μm/min and contains the particles with a diameter of 30 μm, 45 μm and 60 μm. In this regime, cells move faster than without cargo. A possible reason for this is the effect of confinement on the cells. Cells in a confined environment tend to polarize and move with higher velocity then unconfined cells [122, 123]. Due to the higher speed of cells, particle transport is faster as well. In the third regime, particles move at approximately 6 μm/min which is roughly the velocity of the cells without cargo, applying to particles with a diameter of 75 μm. Cells underneath these particles feel a similar confinement effect as cells underneath the 30 μm, 45 μm and 60 μm particles, nevertheless they move much slower. It could be that the particle on the back of the cell is less often moved, since the cell is able to stay in contact with the bead for longer time, as the curvature is much slower.

It is interesting that the drag force seems to have an upper limit. Table 4.2 shows nearly the same value for the mean and the maximum drag force of carrying 60 μm particles and 75 μm particles. This force is very low and below the polymerization force of a single actin filament, which is around 1 pN [124]. Therefore, there seems to be no biological explanation why there are no higher values for the drag force.

The MSD plot shows remarkable differences in the diffusive spreading of the different particles carried by a single cell. The 10 μm particles have the lowest spread, i.e. the slowest growth of the MSD during the observation time. This is in line with the low mean velocity of the particles and the interpretation of cells trying to engulf the beads by phagocytosis. During the process of phagocytosis cells do not move much, resulting in only small net displacement of the bead [121]. The 20 μm particles show a similar diffusive behavior as cells without cargo, although, the mean velocity is slower. A reason could be the different motivations for cells to stay in contact with the cargo. While big cells try to phagocyte the bead, resulting in a slow velocity and only small net displacement over time, small cells feel the particles as a confinement, leading to a mechanically induced polarization. These cells move in a more persistent manner resulting in a higher diffusivity that counterbalances the slowly moving cells in terms of MSD growth. All other particle sizes show a more rapid increase of the MSD than the cells in the controll experiment without a cargo. Nevertheless, there are still unexpected differences between the various types of particles. The strongest MSD growth in figure 4.12 is visible for the 45 μm beads, followed by the 30 μm and 60 μm beads with nearly the same growth. The smallest MSD growth among these particles is reached by the 75 μm beads which diffuse, however, still more rapidly than cells without cargo. The explanation for this different growth patterns goes along with the explanation for the different velocities. With increasing bead size the confinement effect of the particle increases as well. This effect leads to an increased polarization and a more persistent movement of cells. As a result the MSD curves have a higher slope. With increasing particle size the friction increases as well. Since cell forces are limited, the slope of the MSD curves decreases again. In between there is an optimal value due to a treadoff of induced polarization and the slow down by friction at a bead diameter of 45 μm.

The diffusion exponent for the single cells is in line with the value of α in chapter 4.1. The exponent of 0.72 which would indicate a subdiffusive behavior seems to be an error due to the strong slope at the beginning of the curve. It is interesting to see that the diffusion exponent for the 10 and 20 μm particles is the highest ($\alpha = 1.71$). It is questionable whether these particles would be transported most efficiently in terms of MSD for significantly longer tracks.

Bio-hybrid systems based on amoeboid cells are complementary to those based on bacterial swimmers. Amoeboid transporters can withstand perturbations of an advective flow better, since their movement is based on substrate adhesion. On the other hand, bacterial transporters might use the advective transport to reach the desired target faster. Furthermore, the range of cargo size is complementary. A single amoeba can transport cargo which is more than seven times bigger than the cell itself. This exceeds the size which an indiviudal bacterium could carry by far, since it requires several bacteria to propel a micron sized particle [125]. An advantage of using *Dictyostelium* as micro-transport system instead of bacteria is that no surface coating on the particles is needed for the transport. While bio-hybrid systems based on bacteria required the preparation of cargo, e.g. coating,[7–9, 125–127], *Dicyostelium* cells can pick up the cargo without any special treatment.

Furthermore, *Dicyostelium* shares common features with mammalian cells, such as neutrophils or cancer cells [128]. Therefore, the analysis of cargo transport by *Dictyostelium* is a highly interesting problem in the light of bio-hybrid transport in the human body, a first step on the way towards a transport system based on human cells.

5.3 Optical Trap

The setup of the optical trap is comparable to other setups of this kind except for the high powered laser. The wavelength of 1064 nm is quite common. For studying biological samples, it is a good choice to use the near infra-red wavelength range of 750–1100 nm due to the transparency of many biological samples in this wavelength window [86]. Optical traps normally operate with a laser, that has less power [86, 129]. An advantage of our setup is that it is possible to trap bigger particles with this laser and exert stronger forces. However, a disadvantage is that higher laser powers might harm cells.

The experiments revealed detachment forces for the particles up to 330 pN. This is in line with atomic force measurements which revealed mean cell substrate attachment forces of 100 pN [71]. Optical force measurement with particles on living cells have been performed before on melanoma cells, mouse embryo fibroblasts and primary chicken fibroblasts. The measured forces reaches up to 150 pN for particles of 4.5 μm in diameter. The experiments also showed that the forces grow significantly with particle size [129].

In the setup used for the experiments presented here it was not possible to increase the applied forces further since the laser started to harm the cells. A possible reason for cell damage could be the heating of the medium by the laser. Besides the heating of the medium, the cells get damaged as well when the laser energy they are exposed to is too high. Another problem of this technique is the way the bead is pulled out of the trap. The cells did not pull along the focal plane. They normally lifted the particle out of the trap center before they pull it out of the laser beam. As a result they need less force to get the particle out of the trap, than they would need to apply if the particle was moved parallel to the ground.

To overcome these problems in future experiments the technique of magnetic tweezers could be used. Magnetic tweezers do not harm the cells, since magnetic fields do not heat up the buffer. Furthermore, the magnetic tweezers generate isotropic forces [130]. Another option keeping the optical tweezer is the use of particles coupled to each other. In this case the cells pull on one particle while the other one is trapped.

In this way the forces exerted on one particle are transferred to the other particle. In this way cells can stay longer distances away from the laser and the forces on the trapped particle are parallel to the ground.

5.4 Guided Particle Transport

As cells work as transporters for the micro-particles, it is possible to determine the direction of bead movement, by guiding the cell. Under starvation conditions, *Dictyostelium* cells start to aggregate with the help of cAMP signals. Besides this internal system for self assembly it is also possible to guide the cells with an artificial cAMP gradient. While cells follow the signal, they might pick up a particle, resulting in a flow of particles, following the signal as well.

During the experiments showing self-organized particle assembly the distribution of particle distances changes from a one peaked into a bimodal one. The histogram of the initial particle distribution shows a pronounced peak at 0.65 mm. This peak is a result of the limitations of the experimental setup. The field of view has a side length of 1.7 mm. The maximum distance for the particles is given by $\sqrt{2 \cdot (1.7mm)^2} \approx 2.4mm$. The resulting distribution after the cells aggregate has a bimodal shape. The first peak symbolizes the particle distances inside the aggregate, while the second peak displays the distances between the aggregates. This peak is around 1 mm. The results are shown in figure 4.21.

For external guiding two different approaches were used. First a static, linear gradient was established using a commercially available ibidi "μ-Slide Chemotaxis" gradient chamber. One of the reservoirs was filled with phosphate buffer containing 10 μM cAMP and the other one was filled with phosphate buffer only. The ibidi chamber creates a static gradient which lasts for several hours. Cells follow the gradient towards the higher concentration and may eventually pick up a particle on their way, creating a particle flux towards the chamber with the higher cAMP concentration. During movement it could happen that a cell loses the cargo. Eventually another cell picks the bead up again to transport it further. Since, particles do not migrate on their own, i.e. thermal fluctuations are negligible, and every cell is just able to carry one bead, the maximum of the overall particle flux is set by the chemotactic flux of the cells. A problem of this system is that it cannot be changed after initialization. It is neither possible to change the direction of the gradient nor to change its steepness. To create a gradient which can be well detected by the cells, the cAMP concentration at the cAMP reservoir is quite high, which could lead to a saturation of the cAMP receptors of cells and, consequently, to a loss of the chemotactic behavior.

To create a more flexible gradient, photo uncaging was used. Cells where incubated in phosphate buffer containing 10 μM BCMCM-caged cAMP. At first this cell suspension was given into a petri dish together with WGA coated agar particles. A 366 nm laser was focused in the upper left corner of the field of view, resulting in a local release of cAMP and a concentric gradient around the laser spot. Chemotactic cells follow this gradient and drag the beads along. The increasing particle concentration in the vicinity of the laser spot at the end of the experiment in figure 4.23 can be seen as a proof of concept for this technique.

As a next step, cAMP was released inside a dead-end channel of a micro-fluidic system, with the help of photo-uncaging. This experiment is shown in figure 4.24. For this experiment, polystyrene particles with a diameter of 4.5 μm were used. The released cAMP diffuses out of the side branch into the main channel. Cells got attracted and followed the gradient into the side branch. On their way they picked up beads, resulting in a particle stream into the dead-end structure, which is otherwise difficult to achieve. Due to the small size of the cargo, cells carried on average 6 ± 2 particles. As a consequence the particle flux in this experimental setup can be higher than the chemotactic flow of cells.

The technique of photo uncaging is not free of limitations. The bond between the cAMP and the BCMCM may break even without the influence of UV-light. Although the caged compound still worked after a month stored in a fridge, it is self-evident, that all cAMP molecules are still caged by an BCMCM group. On the other hand it is not sure that the laser is breaking the bond between every caged molecule which passes the beam, leading to an unknown steepness of the gradient. Furthermore, the background concentration of cAMP increases over time as more and more caged cAMP is released. In the experiments it was not possible to trigger the laser, as the laser lacked a trigger unit; no shutter could be triggered externally within this setup. Otherwise a periodic release would decrease the problem of increasing background concentrations. A good waiting time between the stimulus would be 6 minutes as this is the natural lag time between cAMP waves for *Dictyostelium* cells. Another problem is the laser itself. UV-light harms living cells [131]; as a result the cells cannot act as transporters anymore after they reached the laser spot. This disadvantage complicates guidance of cells over long distances through a micro-channel system. Furthermore, this way of guidance could not be used for medical applications, as to create a UV-light spot inside the human body. Finally, caged compounds might be not available for chemoattractants of other cells. This could be a problem for future experiments with other types of amoeboid cells.

The guidance of bio-hybrid transport systems has been realized before. Transport assays which rely on molecular motor interaction with cytoskelatal filaments were used, inspired by intracellular transport mechanisms. Several decades ago, it was found that particles coated with molecular motors move along cytoskeletal fibers, like actin filaments or microtubules [132, 133]. This motor-driven translational motion was used later in specific micro-transport assays, for a more detailed review see Refs. [134, 135]. Although initial limitations, like achieving unidirectional transport, could be overcome [136], these motor-driven transport systems require cytoskeletal filaments as predefined tracks, which limits the directional flexibility of their motion compared to cellular micro-transporters. Systems based on bacterial swimmers have been successfully guided by light [7] and chemical gradients [8]. Nevertheless, using amoeboid cells has advantages over bacterial swimmers for guided transport. Unlike *Dictyostelium*, bacteria detect spatial gradients by temporal sensing. When a bacterium senses a positive gradient during a run, the run-time is increased [137, 138]. For more information on bacteria chemotaxis the interested reader is referred to reference [139]. This way of sensing a gradient is less efficient than spatial sensing, since an increase of the chemoattactant concentration over the run length does not indicate to shortest way towards the source, resulting in a small chemotactic index. Furthermore, different mammalian cell types, such as leukocytes, perform amoeboid chemotaxis inside the organism towards an inflammation[140]. This grands the opportunity to use such cells for micro-transport in future medical applications exploiting the natural behavior of cells. It has been already shown, that it is possible to guide bacteria *in vivo* towards a tumor [22]. The same could work for eukaryotic cells. A problem with bacteria as based bio-hybrid transport systems for medical applications is that bacteria itself are often a reason for infections. So it is important that the use of bacteria does not cause more damage for body than help [23]. This problem would be avoided using human specific leukocytes. In this thesis only transport statistics on a planar 2D surface were investigated. This raises the question whether this process would work in a heterogeneous, disordered tissue. The friction on the particle would be much higher such that it may not be possible to carry a cargo on the back of the cell. A possible alternative to carrying the load on the back of the cell is to let the cell phagocyte the load. At the destination the load can be released by a programmable exocytosis.

6

Conclusion and Outlook

This theses demonstrate the potential of *Dictyostelium discoideum* as a promising candidate for bio-hybrid transport. It was shown that cells are able to carry various kinds of particles with no negative effects on the movement of the amoeba. Furthermore, it was possible to guide the cellular micro-trucks with the help of chemical gradients. This can be done exploiting the intrinsic developmentally induced chemotactic aggregation of the cells to build self assembled clusters of the cargo, or by applying an external chemical gradient to guide the cells together with the cargo to a desired location. These findings reveal that motile adherent cells can be used complimentary to swimming bacteria for the transport of micro-cargo. A single amoeba can transport cargo which is more than seven times bigger than the cell itself. This exceeds the size which a bacterium could carry by far. Furthermore, amoeboid transporters can withstand perturbations of an advective flow better, since their movement is based on substrate adhesion. On the other hand, bacterial transporters might use the advective transport to reach the desired target faster.

Although these first steps show the potential of this system, there is still room for investigations. To optimize the transport and avoid unintended loss of the cargo, more detailed knowledge of the adhesion processes in *Dictyostelium discoideum* is necessary. Furthermore, a deeper study of the dynamics of the relevant motor proteins during the transport could help to better understand the behavior of the cells under the influence of different types of cargo.

To take advantage of amoeboid biohybrid transport systems in medical applications, for example as a drug delivery system, it is necessary to test the system in a 3-D matrix, that mimics mammalian tissue. Another critical point is the programmable release of the cargo. So far, cells lose their cargo accidentally. This is not a sufficient option for an inbody use of a drug delivery system, which should keep the cargo attached to the cell until it reaches the target site and release it there. One option for controlled release would be a light-induced cleavage of the cell-cargo bond. Furthermore, cells could carry the cargo particles via phagocytosis. At the destination, the cargo can be released via induced exocytosis.

Although, there are still problems to solve until amoebiod cells can be used reliably as system for drug delivery, this work shows the potential of this approach for the transport of micron-sized cargo.

Appendix

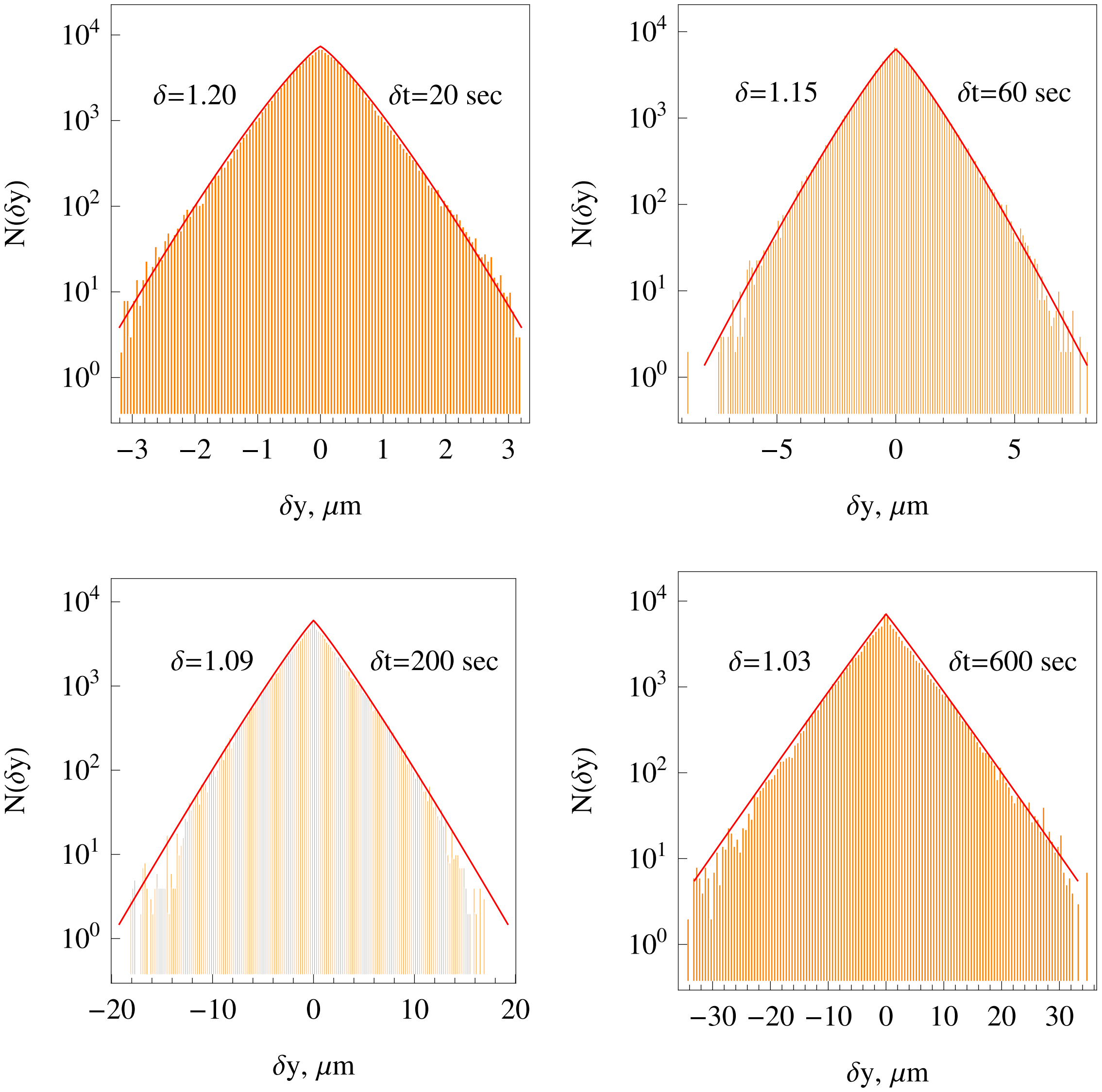

Fig. .1: Log–linear histograms of the number of cell displacements along the y direction for different time-shifts δt, as indicated in the plots. Different horizontal scales in the panels are to be noted. The asymptotes are the blue curves, with the values of the best-fit exponent δ provided in each panel.

Acknowledgement

First of all, I want to thank my parents to put me through collage and support me the whole time.

Second, I would like to thank professor Beta for giving me the opportunity to write my thesis in the biophysics group. For giving me helpful advises during my work, introducing me to the world of science and support during my whole scientific career.

I want to thank all members of the Biological Physics group for the nice working atmosphere. I want to thank especially Marius Hintsche for a lot of scientific discussions and all kinds of MatLab problems. Manuel Frey for helping me with the experiments and Kirsten Sachse for the preparation of the cells for the experiments, otherwise this work would not have been possible.

Furthermore, I want to thank Andrey Cherstvy for helping me with the theoretical analysis and interpretation of the experimental data.

Finally, I would like to thank all the people that accompanied me during my studies, cheered me up in bad times and made this whole time unforgettable.

Bibliography

[1] M. E. Davis, Z. Chen, and D. M. Shin. „Nanoparticle therapeutics: an emerging treatment modality for cancer“. In: *Nature Reviews Drug Discovery* 7.9 (2008), pp. 771–782 (cit. on p. 1).

[2] K. Park. „Facing the truth about nanotechnology in drug delivery“. In: *ACS Nano* 7.9 (2013), pp. 7442–7447 (cit. on p. 1).

[3] H. Rosen and T. Abribat. „The rise and rise of drug delivery“. In: *Nature Reviews Drug Discovery* 4.5 (2005), pp. 381–385 (cit. on p. 1).

[4] Y. H. Bae and K. Park. „Targeted drug delivery to tumors: Myths, reality and possibility“. In: *Journal of Controlled Release* 153.3 (2011), pp. 198–205 (cit. on p. 1).

[5] M. Sitti. „Voyage of the microrobots“. In: *Nature* 458 (2009), p. 2 (cit. on pp. 1, 3).

[6] W. Wang, W. Duan, S. Ahmed, T. E. Mallouk, and A. Sen. „Small power: Autonomous nano- and micromotors propelled by self-generated gradients“. In: *Nano Today* 8.5 (2013), pp. 531–554 (cit. on pp. 1, 3).

[7] D. B. Weibel, P. Garstecki, D. Ryan, et al. „Microoxen: Microorganisms to move microscale loads“. In: *Proceedings of the National Academy of Sciences of the United States of America* 102.34 (2005), pp. 11963–11967 (cit. on pp. 1, 4, 54, 58).

[8] D. Li, H. Choi, S. Cho, et al. „A hybrid actuated microrobot using an electromagnetic field and flagellated bacteria for tumor-targeting therapy“. In: *Biotechnology and bioengineering* 112.8 (2015), pp. 1623–1631 (cit. on pp. 1, 4, 54, 58).

[9] M. M. Stanton, B.-W. Park, D. Vilela, et al. „Magnetotactic bacteria powered biohybrids target *E. coli* biofilms“. In: *ACS Nano* 11.10 (2017), pp. 9968–9978 (cit. on pp. 1, 4, 54).

[10] W. Hu, G. Z. Lum, M. Mastrangeli, and M. Sitti. „Small-scale soft-bodied robot with multimodal locomotion“. In: *Nature* 554.7690 (2018), pp. 81–85 (cit. on p. 3).

[11] W. F. Paxton, K. C. Kistler, C. C. Olmeda, et al. „Catalytic nanomotors: Autonomous movement of striped nanorods“. In: *Journal of the American Chemical Society* 126.41 (2004), pp. 13424–13431 (cit. on p. 3).

[12] L. K. E. A. Abdelmohsen, F. Peng, Y. Tu, and D. A. Wilson. „Micro- and nano-motors for biomedical applications“. In: *J. Mater. Chem. B* 2.17 (2014), pp. 2395–2408 (cit. on p. 3).

[13] Y. Tanaka, K. Sato, T. Shimizu, et al. „A micro-spherical heart pump powered by cultured cardiomyocytes“. In: *Lab Chip* 7.2 (2007), pp. 207–212 (cit. on p. 3).

[14]Y. Tanaka, K. Sato, T. Shimizu, et al. „Demonstration of a bio-microactuator powered by vascular smooth muscle cells coupled to polymer micropillars“. In: *Lab Chip* 8.1 (2008), pp. 58–61 (cit. on p. 3).

[15]A. W. Feinberg, A. Feigel, S. S. Shevkoplyas, et al. „Muscular thin films for building actuators and powering devices“. In: *Science* 317.5843 (2007), pp. 1366–1370 (cit. on p. 3).

[16]K.-I. Kabumoto, T. Hoshino, Y. Akiyama, and K. Morishima. „Voluntary movement controlled by the surface EMG signal for tissue-engineered skeletal muscle on a gripping tool“. In: *Tissue Engineering Part A* 19.15-16 (2013), pp. 1695–1703 (cit. on p. 3).

[17]T. Hoshino, K. Imagawa, Y. Akiyama, and K. Morishima. „Cardiomyocyte-driven gel network for bio mechano-informatic wet robotics“. In: *Biomedical Microdevices* 14.6 (2012), pp. 969–977 (cit. on p. 3).

[18]Y. Akiyama, T. Sakuma, K. Funakoshi, et al. „Atmospheric-operable bioactuator powered by insect muscle packaged with medium“. In: *Lab on a Chip* 13.24 (2013), p. 4870 (cit. on p. 4).

[19]Y. Hiratsuka, M. Miyata, T. Tada, and T. Q. P. Uyeda. „A microrotary motor powered by bacteria“. In: *Proceedings of the National Academy of Sciences* 103.37 (2006), pp. 13618–13623 (cit. on p. 4).

[20]T. Miyamoto, M. Kojima, M. Nakajima, M. Homma, and T. Fukuda. „Rotation of bacteria sheet driven micro gear in open micro channel“. In: *2012 IEEE International Conference on Robotics and Automation*. St Paul, MN, USA: IEEE, 2012, pp. 4080–4085 (cit. on p. 4).

[21]S. Tung and J. W. Kim. „Microscale hybrid devices powered by biological flagellar motors“. In: *IEEE Transactions on Automation Science and Engineering* 3.3 (2006), pp. 260–263 (cit. on p. 4).

[22]S. J. Park, S.-H. Park, S. Cho, et al. „New paradigm for tumor theranostic methodology using bacteria-based microrobot“. In: *Sci Rep* 3 (2013) (cit. on pp. 4, 58).

[23]N. S. Forbes. „Engineering the perfect (bacterial) cancer therapy“. In: *Nature Reviews Cancer* 10.11 (2010), pp. 785–794 (cit. on pp. 4, 58).

[24]D. A. Fletcher and . A. Theriot. „An introduction to cell motility for the physical scientist“. In: *Physical Biology* 1.1 (2004), T1 (cit. on p. 5).

[25]E. Sackmann and R. Merkel. *Lehrbuch der Biophysik*. 1. Auflage. Berlin: WILEY-VCH, Feb. 2010 (cit. on p. 5).

[26]T. D. Pollard and G. G. Borisy. „Cellular motility driven by assembly and disassembly of actin filaments“. In: *Cell* 112.4 (2003), pp. 453–465 (cit. on p. 5).

[27]T. D. Pollard and J. A. Cooper. „Actin, a central player in cell shape and movement“. In: *Science* 326.5957 (2009), pp. 1208–1212 (cit. on p. 5).

[28]L. Hu and G. A. Papoian. „Molecular transport modulates the adaptive response of branched actin networks to an external force“. In: *The Journal of Physical Chemistry B* 117.42 (2013), pp. 13388–13396 (cit. on p. 5).

[29]L. P. Cramer. „Mechanism of cell rear retraction in migrating cells“. In: *Current Opinion in Cell Biology* 25.5 (2013), pp. 591–599 (cit. on p. 5).

[30] R. Ananthakrishnan and A. Ehrlicher. „The forces behind cell movement“. In: *International journal of biological sciences* 3.5 (2007), p. 303 (cit. on p. 6).

[31] A. J. Ridley. „Cell migration: Integrating signals from front to back“. In: *Science* 302.5651 (2003), pp. 1704–1709 (cit. on p. 5).

[32] C. A. Parent. „Making all the right moves: chemotaxis in neutrophils and Dictyostelium“. In: *Current Opinion in Cell Biology* 16.1 (2004), pp. 4–13 (cit. on p. 6).

[33] H. C. Berg and P. M. Tedesco. „Transient response to chemotactic stimuli in Escherichia coli.“ In: *Proceedings of the National Academy of Sciences* 72.8 (1975), pp. 3235–3239 (cit. on p. 6).

[34] L. Song, S. M. Nadkarni, H. U. Bödeker, et al. „Dictyostelium discoideum chemotaxis: Threshold for directed motion“. In: *European Journal of Cell Biology* 85.9-10 (2006), pp. 981–989 (cit. on pp. 6, 21).

[35] Y. Xiong, C.-H. Huang, P. A. Iglesias, and P. N. Devreotes. „Cells navigate with a local-excitation, global-inhibition-biased excitable network“. In: *Proceedings of the National Academy of Sciences* 107.40 (2010), pp. 17079–17086 (cit. on p. 7).

[36] R. Brown. „A brief account of microscopical observations made in the months of June, July and August on the particles contained in the pollen of plants; and on the general existence of active molecules in organic and inorganic bodies“. In: *The Philosophical Magazine* 4.21 (1828), pp. 161–173 (cit. on p. 7).

[37] A. Einstein. „Zur Theorie der Brownschen Bewegung“. In: *Annalen der Physik* 14.S1 (2005), pp. 248–258 (cit. on p. 7).

[38] G. E. Uhlenbeck and L. S. Ornstein. „On the Theory of the Brownian Motion“. In: *Phys Rev* 36.5 (1930), pp. 823–841 (cit. on p. 7).

[39] G. H. Weiss. *Aspects and applications of the random walk*. Amsterdam, The Netherlands: North Holland Press., 1994 (cit. on p. 7).

[40] A. Okubo, J. D. Ackennan, and D. P. Swaney. „Passive Diffusion in Ecosystems“. In: *Journal of Mathematical Biology* 26.3 (1988), pp. 263–298 (cit. on p. 8).

[41] G. Grimmett and D. Stirzaker. *Probability and random processes*. 3rd ed. Oxford ; New York: Oxford University Press, 2001 (cit. on p. 8).

[42] J. D. Murray. *Mathematical biology*. 3rd ed. Interdisciplinary applied mathematics. New York: Springer, 2002 (cit. on p. 8).

[43] H. G. Othmer, R. S. Dunbar, and W. Alt. „Models of dispersal in biological systems“. In: *Journal of Mathematical Biology* 26 (1988), pp. 263–298 (cit. on p. 8).

[44] E. W. Montroll and G. H. Weiss. „Random walks on lattices. II“. In: *Journal of Mathematical Physics* 6.2 (1965), pp. 167–181 (cit. on p. 9).

[45] J. Klafter, A. Blumen, and M. F. Shlesinger. „Stochastic pathway to anomalous diffusion“. In: *Physical Review A* 35.7 (1987), pp. 3081–3085 (cit. on p. 9).

[46] H. Scher, G. Margolin, R. Metzler, J. Klafter, and B. Berkowitz. „The dynamical foundation of fractal stream chemistry: The origin of extremely long retention times: Fractal stream chemistry“. In: *Geophysical Research Letters* 29.5 (2002), pp. 5–1–5–4 (cit. on p. 9).

[47] M. A. Lomholt, T. Ambjörnsson, and R. Metzler. „Optimal target search on a fast-folding polymer chain with volume exchange“. In: *Physical Review Letters* 95.26 (2005) (cit. on p. 9).

[48] R. Metzler and J. Klafter. „The random walk's guide to anomalous diffusion: a fractional dynamics approach“. In: *Physics Reports* 339.1 (2000), pp. 1–77 (cit. on p. 9).

[49] E. A Codling, M. J Plank, and S. Benhamou. „Random walk models in biology“. In: *Journal of The Royal Society Interface* 5.25 (2008), pp. 813–834 (cit. on p. 10).

[50] A. D. Shenderov and M. P. Sheetz. „Inversely correlated cycles in speed and turning in an ameba: an oscillatory model of cell locomotion“. In: *Biophysical Journal* 72.5 (1997), pp. 2382–2389 (cit. on pp. 10, 52).

[51] H. U. Bödeker, C. Beta, T. D. Frank, and E. Bodenschatz. „Quantitative analysis of random ameboid motion“. In: *EPL (Europhysics Letters)* 90.2 (2010), p. 28005 (cit. on p. 10).

[52] Gabriel Amselem, Matthias Theves, Albert Bae, Eberhard Bodenschatz, and Carsten Beta. „A Stochastic Description of Dictyostelium Chemotaxis“. In: *PLoS ONE* 7.5 (May 2012), e37213 (cit. on p. 10).

[53] Natallia Makarava, Stephan Menz, Matthias Theves, et al. „Quantifying the degree of persistence in random amoeboid motion based on the Hurst exponent of fractional Brownian motion“. In: *Physical Review E* 90.4 (Oct. 2014), p. 042703 (cit. on p. 10).

[54] K. B. Raper. „Dictyostelium discoideum, a new species of slime mold from decaying forest leaves“. In: *Journal of agricultural research* 50.2 (1935), p. 135–147. (Cit. on p. 10).

[55] L. Eichinger, J. A. Pachebat, G. Glöckner, et al. „The genome of the social amoeba Dictyostelium discoideum“. In: *Nature* 435.7038 (2005), pp. 43–57 (cit. on pp. 10, 14).

[56] R. H. Kessin. *Dictyostelium*. Developmental and Cell Biology. Cambridge University Press, 2001 (cit. on pp. 10–12).

[57] G. Gerisch. „Periodische Signale steuern die Musterbildung in Zellverbänden“. In: *Naturwissenschaften* 58.9 (1971), pp. 430–438 (cit. on p. 11).

[58] O. Hazeki, T. Okada, H. Kurosu, et al. „Activation of PI 3-kinase by G protein $\beta\gamma$ subunits“. In: *Life sciences* 62.17 (1998), pp. 1555–1559 (cit. on p. 12).

[59] F. I. Comer and C. A. Parent. „PI 3-kinases and PTEN: how opposites chemoattract“. In: *Cell* 109.5 (2002), pp. 541–544 (cit. on p. 12).

[60] C. A. Parent, B. J. Blacklock, W. M. Froehlich, D. B. Murphy, and P. N. Devreotes. „G protein signaling events are activated at the leading edge of chemotactic cells“. In: *Cell* 95.1 (1998), pp. 81–91 (cit. on p. 12).

[61] A. Bagorda and C. A. Parent. „Eukaryotic chemotaxis at a glance“. In: *Journal of Cell Science* 121.16 (2008), pp. 2621–2624 (cit. on p. 12).

[62] A. Kortholt, R. Kataria, I. Keizer-Gunnink, et al. „Dictyostelium chemotaxis: essential Ras activation and accessory signalling pathways for amplification“. In: *EMBO reports* 12.12 (2011), pp. 1273–1279 (cit. on pp. 12, 13).

[63]Y. Kamimura, Y. Xiong, P. A. Iglesias, et al. „PIP3-independent activation of TorC2 and PKB at the cell's leading edge mediates chemotaxis“. In: *Current Biology* 18.14 (2008), pp. 1034–1043 (cit. on p. 12).

[64]D. M. Veltman, I. Keizer-Gunnik, and P. J.M. Van Haastert. „Four key signaling pathways mediating chemotaxis in Dictyostelium discoideum“. In: *The Journal of Cell Biology* 180.4 (2008), pp. 747–753 (cit. on p. 12).

[65]H. Lodish, A. Berk, C. A. Kaiser, et al. *Molecular cell biology*. 6th ed. New York: W. H. Freeman and Company, 2008 (cit. on p. 13).

[66]B. Alberts, A. Johnson, J. Lewis, et al. *Molecular biology of the cell*. 5th ed. Garland Science, 2008 (cit. on p. 13).

[67]A. Sebe-Pedros, A. J. Roger, F. B. Lang, N. King, and I. Ruiz-Trillo. „Ancient origin of the integrin-mediated adhesion and signaling machinery“. In: *Proceedings of the National Academy of Sciences* 107.22 (2010), pp. 10142–10147 (cit. on p. 14).

[68]P. Fey, S. Stephens, M. A. Titus, and R. L. Chisholm. „SadA, a novel adhesion receptor in *Dictyostelium*“. In: *The Journal of Cell Biology* 159.6 (2002), pp. 1109–1119 (cit. on p. 14).

[69]S. Cornillon, E. Pech, M. Benghezal, et al. „Phg1p is a nine-transmembrane protein superfamily member involved in *Dictyostelium* adhesion and phagocytosis“. In: *Journal of Biological Chemistry* 275.44 (2000), pp. 34287–34292 (cit. on p. 14).

[70]J. Niewöhner, I. Weber, M. Maniak, A. Müller-Taubenberger, and G. Gerisch. „Talin-Null cells of *Dictyostelium* are strongly defective in adhesion to particle and substrate surfaces and slightly impaired in cytokinesis“. In: *The Journal of Cell Biology* 138.2 (1997), pp. 349–361 (cit. on p. 14).

[71]M. Tarantola, A. Bae, D. Fuller, et al. „Cell substratum adhesion during early development of dictyostelium discoideum“. In: *PLoS ONE* 9.9 (2014), e106574 (cit. on pp. 14, 55).

[72]N. Ibarra, S. L. Blagg, F. Vazquez, and R. H. Insall. „Nap1 regulates Dictyostelium cell motility and adhesion through SCAR-dependent and -independent pathways“. In: *Current Biology* 16.7 (2006), pp. 717–722 (cit. on p. 14).

[73]S. Cornillon, R. Froquet, and P. Cosson. „Involvement of Sib proteins in the regulation of cellular adhesion in Dictyostelium discoideum“. In: *Eukaryotic Cell* 7.9 (2008), pp. 1600–1605 (cit. on p. 14).

[74]T. R. Varney, E. Casademunt, H. N. Ho, et al. „A novel Dictyostelium gene encoding multiple repeats of adhesion inhibitor-like domains has effects on cell–cell and cell–substrate adhesion“. In: *Developmental Biology* 243.2 (2002), pp. 226–248 (cit. on p. 14).

[75]T. J. Lampert, N. Kamprad, M. Edwards, et al. „Shear force-based genetic screen reveals negative regulators of cell adhesion and protrusive activity“. In: *Proceedings of the National Academy of Sciences* 114.37 (2017), E7727–E7736 (cit. on p. 14).

[76]W. F. Loomis, D. Fuller, E. Gutierrez, A. Groisman, and W.-J. Rappel. „Innate non-specific cell substratum adhesion“. In: *PLoS ONE* 7.8 (2012), e42033 (cit. on p. 14).

[77]E. Decave. „Shear flow-induced motility of Dictyostelium discoideum cells on solid substrate“. In: *Journal of Cell Science* 116.21 (2003), pp. 4331–4343 (cit. on p. 14).

[78]I. Weber, E. Wallraff, R. Albrecht, and G. Gerisch. „Motility and substratum adhesion of Dictyostelium wild-type and cytoskeletal mutant cells: a study by RICM/bright-field double-view image analysis“. In: *Journal of Cell Science* 108 (1995), pp. 1519–1530 (cit. on p. 14).

[79]H. Clausen-Schaumann, M. Seitz, R. Krautbauer, and H. E. Gaub. „Force spectroscopy with single bio-molecules“. In: *Current Opinion in Chemical Biology* 4.5 (2000), pp. 524–530 (cit. on p. 14).

[80]S. M. Block and K. Svoboda. „Analysis of high resolution recordings of motor movement“. In: *Biophysical Journal* 68 (1995), p. 10 (cit. on p. 14).

[81]M. Aspholm, A. Kalia, S. Ruhl, et al. „Helicobacter pylori adhesion to carbohydrates“. In: *Methods in Enzymology*. Vol. 417. Elsevier, 2006, pp. 293–339 (cit. on p. 14).

[82]M. D. Wang, H. Yin, R. Landick, J. Gelles, and S. M. Block. „Stretching DNA with optical tweezers“. In: *Biophysical Journal* 72.3 (1997), pp. 1335–1346 (cit. on pp. 14, 18).

[83]A. Ashkin, J. M. Dziedzic, J. E. Bjorkholm, and S. Chu. „Observation of a single-beam gradient force optical trap for dielectric particles“. In: *Optics letters* 11.5 (1986), pp. 288–290 (cit. on p. 15).

[84]A. Ashkin, J. M. Dziedzic, and T. Yamane. „Optical trapping and manipulation of single cells using infrared laser beams“. In: *Nature* 330 (1987), pp. 769–771 (cit. on p. 15).

[85]A. Ashkin. „Optical trapping and manipulation of neutral particles using lasers“. In: *Proc. Natl. Acad. Sci. USA* (1997), p. 8 (cit. on p. 15).

[86]K. Dholakia, P. Reece, and M. Gu. „Optical micromanipulation“. In: *Chem. Soc. Rev.* 37.1 (2008), pp. 42–55 (cit. on pp. 15, 55).

[87]M. Daly, M. Sergides, and S. Nic Chormaic. „Optical trapping and manipulation of micrometer and submicrometer particles: Optical trapping and manipulation of micrometer and submicrometer particles“. In: *Laser & Photonics Reviews* 9.3 (2015), pp. 309–329 (cit. on p. 15).

[88]Y. Harada and T. Asakura. „Radiation forces on a dielectric sphere in the Rayleigh scattering regime“. In: *Optics Communications* 124.5-6 (1996), pp. 529–541 (cit. on pp. 15, 16).

[89]T. A. Nieminen, G. Knöner, N. R. Heckenberg, and H. Rubinsztein-Dunlop. „Physics of optical tweezers“. In: *Methods in Cell Biology*. Vol. 82. Elsevier, 2007, pp. 207–236 (cit. on p. 16).

[90]J. A. Lock and G. Gouesbet. „Generalized Lorenz–Mie theory and applications“. In: *Journal of Quantitative Spectroscopy and Radiative Transfer* 110.11 (2009), pp. 800–807 (cit. on p. 16).

[91]H. Yin, M. D. Wang, K. Svoboda, et al. „Transcription against an applied force“. In: *Science* 270 (1995), p. 6 (cit. on p. 18).

[92]P.J. Bronkhorst, G.J. Streekstra, J. Grimbergen, et al. „A new method to study shape recovery of red blood cells using multiple optical trapping“. In: *Biophysical Journal* 69.5 (1995), pp. 1666–1673 (cit. on p. 18).

[93] G. Sinclair, P. Jordan, J. Courtial, et al. „Assembly of 3-dimensional structures using programmable holographic optical tweezers“. In: *Optics Express* 12.22 (2004), p. 5475 (cit. on p. 18).

[94] D. G. Grier. „A revolution in optical manipulation“. In: *Nature* 424.6950 (2003), pp. 810–816 (cit. on p. 18).

[95] K. Jacobs, R. Seemann, and H. Kuhlmann. „Mikrofluidik“. In: *Physikalische Chemie* 53 (2005), pp. 300–304 (cit. on p. 18).

[96] N.-T. Nguyen. *Mikrofluidik Entwurf, Herstellung und Charakterisierung*. Wiesbaden: B.G. Teudner Verlag/ GWV Fachverlage GmbH, 2004 (cit. on p. 18).

[97] D. C. Duffy, J. C. McDonald, O. J. A. Schueller, and G. M. Whitesides. „Rapid prototyping of microfluidic systems in poly(dimethylsiloxane)“. In: *Analytical Chemistry* 70.23 (1998), pp. 4974–4984 (cit. on p. 19).

[98] Carsten Beta. „Spatiotemporal Stimulation of Single Cells Using Flow Photolysis“. In: *Chemotaxis*. Ed. by Tian Jin and Dale Hereld. Vol. 571. Totowa, NJ: Humana Press, 2009, pp. 321–332 (cit. on p. 19).

[99] O. Nagel. *Untersuchung des Einflusses der Umgebungsgeometrie auf spontane Zellbewegung*. Sept. 2011 (cit. on p. 20).

[100] Gabriel Amselem, Matthias Theves, Albert Bae, Carsten Beta, and Eberhard Bodenschatz. „Control Parameter Description of Eukaryotic Chemotaxis“. In: *Physical Review Letters* 109.10 (Sept. 2012), p. 108103 (cit. on p. 21).

[101] R. P. Futrelle. „Dictyostelium chemotactic response to spatial and temporal gradients. Theories of the limits of chemotactic sensitivity and of pseudochemotaxis“. In: *Journal of cellular biochemistry* 18.2 (1982), pp. 197–212 (cit. on p. 22).

[102] V. Hagen, J. Bendig, S. Frings, et al. „Highly efficient and ultrafast phototriggers for cAMP and cGMP by using long-wavelength UV/VIS-activation“. In: *Angewandte Chemie International Edition* 40.6 (2001), pp. 1045–1048 (cit. on p. 22).

[103] J. M. Nerbonne, S. Richard, J. Nargeot, and H. A. Lester. „New photoactivatable cyclic nucleotides produce intracellular jumps in cyclic AMP and cyclic GMP concentrations“. In: *Nature* 310 (1984), pp. 74–76 (cit. on p. 22).

[104] Carsten Beta, Danica Wyatt, Wouter-Jan Rappel, and Eberhard Bodenschatz. „Flow Photolysis for Spatiotemporal Stimulation of Single Cells“. In: *Analytical Chemistry* 79.10 (May 2007), pp. 3940–3944 (cit. on p. 23).

[105] Carsten Beta and Eberhard Bodenschatz. „Microfluidic tools for quantitative studies of eukaryotic chemotaxis“. In: *European Journal of Cell Biology* 90.10 (Oct. 2011), pp. 811–816 (cit. on p. 23).

[106] J. C. Crocker and D. G. Grier. „Methods of digital video microscopy for colloidal studies“. In: *Journal of colloid and interface science* 179.1 (1996), pp. 298–310 (cit. on p. 24).

[107] M. Theves. *Diploma Thesis Quantitative Study of Eukaryotic Chemotaxis with Microfluidic Devices*. 2009 (cit. on p. 24).

[108]A. G. Cherstvy, O. Nagel, C. Beta, and R. Metzler. „Non-Gaussianity, population heterogeneity, and transient superdiffusion in the spreading dynamics of amoeboid cells“. In: *Phys. Chem. Chem. Phys.* 20.35 (2018), pp. 23034–23054 (cit. on pp. 27–30, 32, 35–37).

[109]L. Li, S. F. Nørrelykke, and E. C. Cox. „Persistent cell motion in the absence of external signals: A search strategy for eukaryotic cells“. In: *PLoS ONE* 3.5 (2008), e2093 (cit. on pp. 30, 51, 52).

[110]J. N. Pedersen, L. Li, C. Grădinaru, et al. „How to connect time-lapse recorded trajectories of motile microorganisms with dynamical models in continuous time“. In: *Phys. Rev. E* 94.6 (2016) (cit. on p. 30).

[111]A. S. Bodrova, A. V. Chechkin, A. G. Cherstvy, et al. „Underdamped scaled Brownian motion: (non-)existence of the overdamped limit in anomalous diffusion“. In: *Scientific Reports* 6.1 (Sept. 2016) (cit. on p. 32).

[112]R. Metzler, J.-H. Jeon, A. G. Cherstvy, and E. Barkai. „Anomalous diffusion models and their properties: non-stationarity, non-ergodicity, and ageing at the centenary of single particle tracking“. In: *Phys. Chem. Chem. Phys.* 16.44 (2014), pp. 24128–24164 (cit. on p. 51).

[113]L. G. A. Alves, D. B. Scariot, R. R. Guimarães, et al. „Transient superdiffusion and long-range correlations in the motility patterns of trypanosomatid flagellate protozoa“. In: *PLOS ONE* 11.3 (2016), e0152092 (cit. on pp. 51, 52).

[114]T. Wagner, A. Kroll, C. R. Haramagatti, H.-G. Lipinski, and M. Wiemann. „Classification and segmentation of nanoparticle diffusion trajectories in cellular micro environments“. In: *PLOS ONE* 12.1 (2017), e0170165 (cit. on p. 51).

[115]D. A. Brock, T. E. Douglas, D. C. Queller, and J. E. Strassmann. „Primitive agriculture in a social amoeba“. In: *Nature* 469.7330 (2011), pp. 393–396 (cit. on p. 51).

[116]L. Golé, C. Rivière, Y. Hayakawa, and J.-P. Rieu. „A quorum-sensing factor in vegetative Dictyostelium discoideum cells revealed by quantitative migration analysis“. In: *PLoS ONE* 6.11 (2011), e26901 (cit. on p. 52).

[117]D. Selmeczi, L. Li, L. I. I. Pedersen, et al. „Cell motility as random motion: A review: Cell motility as random motion“. In: *The European Physical Journal Special Topics* 157.1 (2008), pp. 1–15 (cit. on p. 52).

[118]M. J. Potel and S. A. Mackay. „Preaggregative cell motion in Dictyostelium“. In: *Journal of Cell Science* 36 (1979), pp. 281–309 (cit. on p. 52).

[119]J.-H. Jeon, V. Tejedor, S. Burov, et al. „In vivo anomalous diffusion and weak ergodicity breaking of lipid granules“. In: *Physical Review Letters* 106.4 (2011) (cit. on p. 52).

[120]D. Arcizet, S. Capito, M. Gorelashvili, et al. „Contact-controlled amoeboid motility induces dynamic cell trapping in 3D-microstructured surfaces“. In: *Soft Matter* 8.5 (2012), p. 1473 (cit. on p. 52).

[121]J. R. Chubb. „The Dictyostelium RasS protein is required for macropinocytosis, phagocytosis and the control of cell movement“. In: *Journal of Cell Science* 113.4 (2000), pp. 709–719 (cit. on pp. 53, 54).

[122]R. Hawkins, M. Piel, G. Faure-Andre, et al. „Pushing off the Walls: A mechanism of cell motility in confinement“. In: *Physical Review Letters* 102.5 (2009) (cit. on p. 53).

[123]O. Nagel, C. Guven, M. Theves, et al. „Geometry-driven polarity in motile amoeboid cells“. In: *PLoS ONE* 9.12 (2014), e113382 (cit. on p. 53).

[124]M. J. Footer, J. W. J. Kerssemakers, J. A. Theriot, and M. Dogterom. „Direct measurement of force generation by actin filament polymerization using an optical trap“. In: *Proceedings of the National Academy of Sciences* 104.7 (2007), pp. 2181–2186 (cit. on p. 53).

[125]Z. Hosseinidoust, B. Mostaghaci, O. Yasa, et al. „Bioengineered and biohybrid bacteria-based systems for drug delivery“. In: *Advanced Drug Delivery Reviews* 106 (2016), pp. 27–44 (cit. on p. 54).

[126]A. V. Singh, Z. Hosseinidoust, B.-W. Park, O. Yasa, and M. Sitti. „Microemulsion-based soft bacteria-driven microswimmers for active cargo delivery“. In: *ACS Nano* 11.10 (2017), pp. 9759–9769 (cit. on p. 54).

[127]B.-W. Park, J. Zhuang, O. Yasa, and M. Sitti. „Multifunctional bacteria-driven microswimmers for targeted active drug delivery“. In: *ACS Nano* 11.9 (2017), pp. 8910–8923 (cit. on p. 54).

[128]A. Müller-Taubenberger, A. Kortholt, and L. Eichinger. „Simple system – substantial share: The use of Dictyostelium in cell biology and molecular medicine“. In: *European Journal of Cell Biology* 92.2 (2013), pp. 45–53 (cit. on p. 55).

[129]M. Schwingel and M. Bastmeyer. „Force mapping during the formation and maturation of cell adhesion sites with multiple optical tweezers“. In: *PLoS ONE* 8.1 (2013). Ed. by F. Frischknecht, e54850 (cit. on p. 55).

[130]A. R. Bausch, F. Ziemann, A. A. Boulbitch, K. Jacobson, and E. Sackmann. „Local measurements of viscoelastic parameters of adherent cell surfaces by magnetic bead microrheometry“. In: *Biophysical Journal* 75.4 (1998), pp. 2038–2049 (cit. on p. 55).

[131]R. R. Marshall, C. F. Arlett, S. A. Harcourt, and B. A. Broughton. „Increased sensitivity of cell strains from Cockayne’s syndrome to sister-chromatid-exchange induction and cell killing by UV light“. In: *Mutation Research/Fundamental and Molecular Mechanisms of Mutagenesis* 69.1 (1980), pp. 107–112 (cit. on p. 57).

[132]M. P. Sheetz and J. A. Spudich. „Movement of myosin-coated flurescent beads on actin cables in vitro“. In: *Nature* 303 (1983), pp. 31–35 (cit. on p. 58).

[133]R. D. Allen. „Gliding movement of and bidirectional transport along single native microtubules from squid axoplasm: evidence for an active role of microtubules in cytoplasmic transport“. In: *The Journal of Cell Biology* 100.5 (1985), pp. 1736–1752 (cit. on p. 58).

[134]H. Hess and V. Vogel. „Molecular shuttles based on motor proteins: active transport in synthetic environments“. In: *Reviews in Molecular Biotechnology* 82.1 (2001), pp. 67–85 (cit. on p. 58).

[135]H. Hess. „Engineering Applications of Biomolecular Motors“. In: *Annual Review of Biomedical Engineering* 13.1 (2011), pp. 429–450 (cit. on p. 58).

[136]K. J. Böhm, R. Stracke, P. Mühlig, and E. Unger. „Motor protein-driven unidirectional transport of micrometer-sized cargoes across isopolar microtubule arrays“. In: *Nanotechnology* 12.3 (2001), pp. 238–244 (cit. on p. 58).

[137]J. Adler. „Motile Escherichia coli migrate in bands that are influenced by oxygen and organic nutrients.“ In: *Science* 153 (1966), pp. 708–716 (cit. on p. 58).

[138]D. A. Brown and H. C. Berg. „Temporal Stimulation of Chemotaxis in Escherichia coli“. In: *Proceedings of the National Academy of Sciences* 71.4 (1974), pp. 1388–1392 (cit. on p. 58).

[139]G. H. Wadhams and J. P. Armitage. „Making sense of it all: bacterial chemotaxis“. In: *Nature Reviews Molecular Cell Biology* 5.12 (2004), pp. 1024–1037 (cit. on p. 58).

[140]S. H. Zigmond. „Leukocyte locomotion and chemotaxis: New methods for evaluation, and demonstration of a cell-driven chemotactic factor“. In: *Journal of Experimental Medicine* 137.2 (1973), pp. 387–410 (cit. on p. 58).

List of Figures

List of Tables

Declaration

I hereby declare that I have completed the work solely and only with the help of the mentioned references.

Potsdam, June 1, 2019

Oliver Nagel